Obesogenic Diet Impairs Social Memory Through Alterations of Hippocampal CA2 Excitability and Oxytocin Signaling

Maud Muller[1], Alice Fermigier[3], Eva Ducourneau[3], Arielle Rakotonandrasana[3], Guillaume Ferreira[3], Vivien Chevaleyre[1,2,4,5] and Rebecca A Piskorowski[1,2,4,5,6]

[1]Université Paris Cité, Institute of Psychiatry and Neuroscience of Paris (IPNP), INSERM U1266, Team Synaptic Plasticity and Neural Networks, 75014 Paris, France

[2]GHU-Paris Psychiatrie et Neurosciences, Hôpital Sainte Anne, F-75014 Paris, France

[3] University of Bordeaux, INRAE, Bordeaux INP, NutriNeuro, UMR 1286, F-33077, Bordeaux, France

[4] Sorbonne Université, CNRS, Inserm, Center for Neuroscience at Sorbonne Université (NeuroSU), F-75005 Paris, France

[5]Sorbonne Université, CNRS, Inserm, Institut de Biologie Paris-Seine (IBPS), F75005 Paris, France

[6]Corresponding author: RA Piskorowski, rebecca.piskorowski@inserm.fr

Keywords: High-Fat Diet, Hippocampal area CA2, Oxytocin, Synaptic plasticity, Social Recognition Memory

ABSTRACT

While obesity induces cardio-metabolic disorders and cognitive deficits, the underlying neural mechanisms remain unexplored. In mice, exposure to an obesogenic high-fat and sugar diet (HFD) resulted in social recognition memory deficits, a process that is dependent upon hippocampal area CA2 and oxytocin signaling. HFD-fed mice had stronger inputs onto CA2 pyramidal neurons that led to increased action potential firing, without altering intrinsic properties or inhibitory transmission. Chemogenetic CA2 inhibition rescued HFD-induced social memory deficits, confirming the role of CA2 hyperexcitability in these effects. In CA2, oxytocin receptor activation resulted in membrane depolarization, spontaneous action-potential firing and permitted endocannabinoid-mediated plasticity in control diet-fed mice, but not HFD-fed littermates. In a concentration-dependent manner, oxytocin restored potentiation of excitatory responses and allowed for endocannabinoid plasticity at CA2 inhibitory synapses as well as social memory deficits in HFD-fed mice. By investigating the influence of diet on hippocampal area CA2, this study uncovers novel mechanisms linking neuromodulation and plasticity in social memory encoding.

INTRODUCTION

Nearly half of the global population and almost 20% of children and adolescents are overweight or obese. While these levels seem to be plateauing in high-income countries, global obesity levels are increasing in both young and adult populations (Chooi et al., 2019; Alfaris et al., 2023). Excessive caloric intake, particularly from western diets rich in saturated fat and refined sugar is a pivotal driver of this epidemic (Blüher, 2019). While the adverse metabolic consequences, cardiovascular risks, and the oncogenic potential of obesity are well-documented, the impact on cognitive function remains comparatively unexplored. Nonetheless, clinical studies have reported adverse effects of obesity or western diets on cognition (for reviews: Martin and Davidson, 2014; Yeomans, 2017) and learning and memory performance (Loprinzi and Frith, 2018). With this evidence, the underlying mechanisms related to these changes are unexplored.

Amongst widespread impairments in cognition, rodents fed an obesogenic diet, have been reported to undergo hippocampal learning and memory deficits (for reviews: Cordner and Tamashiro, 2015; Abbott et al., 2019; Tsan et al., 2021; Fadó et al., 2022). Interestingly, social recognition memory (SRM) has been shown to be impaired following exposure to an obesogenic high-fat and sugar diet (HFD) (Takase et al., 2016; Reichelt et al., 2019; Yaseen et al., 2019; Hayashi et al., 2020; Wu et al., 2023). Area CA2 of the dorsal hippocampus (dCA2) has been shown by targeted lesions, chemogenetic and optogenetic studies to play a central role in SRM (Hitti and Siegelbaum, 2014; Stevenson and Caldwell, 2014; Meira et al., 2018; Oliva et al., 2020). With this, afferents from the lateral entorhinal cortex (EC), hypothalamic paraventricular nucleus (PVN), supramammillary nucleus and septum have been proven necessary for SRM (Lin et al., 2018; Chen et al., 2020; Pimpinella et al., 2021; Lopez-Rojas et al., 2022). Interestingly, oxytocin (OT), a prosocial neuropeptide, seems to regulate dCA2 function. Specifically, dCA2 pyramidal neurons (PNs) express OT receptors (OTR), that, when activated result in increased excitability and spontaneous burst firing of CA2 PNs (Tirko et al., 2018) and also in a synaptic potentiation at the CA3-CA2 and EC-CA2 glutamatergic synapses (Pagani et al., 2014; Lin et al., 2018). OT inputs from the PVN have been shown to be important for SRM (Raam et al., 2017; Lin et al., 2018; Tsai et al., 2022). It is known though, that disruption in OT signaling is associated with obesity. OT plays a role in appetite suppression, has been shown to modulate food intake (Kerem and Lawson, 2021) and studies have reported changes in plasma OT concentrations in obese individuals (Kerem and Lawson, 2021). In HFD-induced obese mice, reduction of blood OT concentrations has been

documented (Zhang and Cai, 2011), alongside a decrease in OT signaling in the hippocampus (Hayashi et al., 2020; Khazen et al., 2022). Additionally, the endocannabinoid (eCB) system has been highlighted as a key player in the pathogenesis of obesity (Di Marzo, 2008) and exposure to a HFD has been reported to alter endocannabinoid signaling in the hippocampus (Massa et al., 2010; Rivera et al., 2013). In area CA2, eCB-mediated inhibitory long-term depression (iLTD) of GABAergic inputs onto CA2 PNs has been shown to be required for SRM in standard diet-fed mice (Loisy et al., 2022). Thus, the exposure to HFD may be altering the function of CA2 by two separate mechanisms: eCB and OT signaling.

To understand the mechanisms underlying SRM deficits in HFD-fed mice, we examined synaptic transmission in area CA2, its OT signaling and eCB-mediated plasticity of GABAergic transmission. We provide evidence that the CA2 PNs of HFD-fed mice are hyperexcitable and chemogenetic inhibition of these cells is sufficient to resolve SRM deficits. Furthermore, we show that OT-induced potentiation of excitatory responses onto CA2 PNs is impaired in HFD-fed mice and that OT signaling in area CA2 is permissive for the eCB plasticity in control conditions but disrupted under HFD exposure. Higher concentrations of OT restored potentiation of excitatory responses and allowed for endocannabinoid plasticity at CA2 glutamatergic synapses in slices prepared from HFD-fed mice. CA2 infusion of OT, in a concentration-dependent manner, rescued SRM deficits in HFD-fed mice.

RESULTS

HFD exposure induces SRM impairments

To determine how exposure to an obesogenic diet compromises physiology and hippocampal-dependent SRM, we exposed male and female mice to a HFD consisting of 45% kcal from saturated fat for 12 weeks just after weaning at 21 days. This exposure lasted until mice were 15 weeks-old, an age that is considered to be adulthood (Dutta and Sengupta, 2016). This exposure to HFD induced significant weight gain and increased fat mass in both male and female mice (Sup Fig 1A-C). Shorter periods of exposure to the HFD of 10 days and 5 weeks did not result in significant weight gain.

To assess the effect of adolescent HFD exposure on SRM, we adapted a social discrimination test (from (Okuyama et al., 2016; Rani et al., 2021) using 15 minutes and 3-hour delay between training and test (Fig 1A). To first examine sociability during training, we compared

the exploration time of a novel social conspecific in a small cage, versus the same empty cage. Both groups explored more the social stimulus (Fig 1B, CD: n=16, HFD: n=15, $p<0.001$ comparison with 50%) and exhibited a sociability index higher than 0 (Fig 1C; $p<0.001$) indicating normal sociability. Memory for the stimulus mouse was tested in both groups either 15 minutes or 3 hours later (Fig 1D-E). While both CD- and HFD-fed mice explored the novel stimulus mouse more than the familiar one after 15 minutes (CD: n=15, $p<0.05$; HFD: n=10, $p<0.05$), only CD-fed mice showed similar performance after 3 hours (CD: n=16, $p<0.01$) whereas the mice exposed to a HFD did not discriminate between the familiar and novel mice (HFD: n=15, $p>0.1$). The fact that HFD-fed mice succeeded in discriminating between familiar and novel mouse after a 15 min delay excludes any sensory, motor, motivational or attentional alterations that could interfere with the discrimination performance and indicates a specific effect of HFD on memory.

dCA2 excitability is enhanced following a HFD

As hippocampal area CA2 activity is required for SRM, we hypothesized that a HFD may induce alterations in this area that could lead to deficits in SRM. In order to test this, we used transverse hippocampal slices of HFD-fed and CD-fed mice and measured synaptic transmission in area CA2. Upon stimulation of Schaffer collateral (SC) afferents, field post-synaptic potentials recorded in stratum radiatum of area CA2 were larger in the HFD-fed group compared to the CD-fed group (Fig 1F, CD: n=13,6; HFD: n=23,10, p=0.0015), after normalizing to fiber volley (HFD: n=23,10, CD: n=13,6; p=0.016). We performed whole-cell recordings of CA2 PNs to directly examine changes in synaptic transmission at the CA3-CA2 synapse. In slices prepared from HFD-fed mice, we observed a consistent increase in the amplitude of post-synaptic potentials with SC stimulation (Fig 1G, HFD: n=34,18; CD: n=23,17; p=0.0052 for diet effect stimulation 1; p= 0.014 for diet effect stimulation 2).

To determine how much of this difference was due to inhibitory and excitatory transmission, we performed whole-cell voltage-clamp recordings to monitor inhibitory post synaptic potentials (IPSCs) at +10 mV both with and without AMPA and NMDA receptor blockers (NBQX and APV). No significant difference in the amplitude of IPSCs were observed between groups when we measured both feedforward inhibition (Sup Fig 2A, CD: n=18,11; HFD: n=17,12; p=0.086 for diet effect of stimulation 1; p=0.41 for diet effect of stimulation 2) or direct inhibition onto CA2 PNs (Sup Fig 2B, CD: n=18,11; HFD: n=17,12; p=0.40 for diet effect of stimulation 1; p= 0.12 for diet effect of stimulation 2). However, a decrease of

the inhibitory paired-pulse ratio (PPR) of two subsequent IPSCs was observed in the HFD group (Sup Fig 2C, CD: n=18,11; HFD: n=17,12; p= 0.041 for diet effect), possibly indicating a change in presynaptic properties of GABA release in area CA2. Neither the amplitude not the frequency of spontaneous inhibitory activity onto area CA2 in the presence or absence of excitatory transmission blockers was altered by a HFD (Sup Fig 2D-G).

As inhibitory transmission onto CA2 was mostly unaltered by 12 weeks of a HFD, we measured the strength of excitatory transmission via patch-clamp recordings of CA2 PNs maintained at -70 mV in the presence of $GABA_A$ and $GABA_B$ receptor blockers (SR95531 and CGP55845). HFD exposure enhanced the strength of excitatory transmission onto CA2 PNs evoked by SC stimulation (Fig 1H**,** CD: n=9,4; HFD: n=8,3; p=0.0064 for diet effect stimulation 1; p=0.014 for diet effect stimulation 2). When we examined the ratio of the second evoked EPSP amplitude to the first, the ratio for the HFD-fed group was significantly lower as compared to the CD-fed group (Fig 1H, CD: n=9,4; HFD: n=8,3; p=0.0041 for diet effect). A reduction in PPR indicates that the probability of glutamate release at the CA3-CA2 synapse may be increased by 12 weeks of HFD.

To verify if the hyperexcitability of area CA2 influences the probability of CA2 PN AP firing, we performed field recordings to record population spikes (PS) in the somatic layer of area CA2 upon SC stimulation. Stimulation of this input induced strong population-level AP firing of CA2 PNs in HFD-fed mice while stimulation of these inputs barely allowed for AP firing in control-diet mice, (Fig 1I**,** CD: n=18,7; HFD: n=23,6; p= 2.2E-4 for diet effect of stimulation 1; p= 7.4E-6 for diet effect of stimulation 2).

Because cortical input to area CA2 is also important for SRM (Lopez-Rojas et al., 2022) and can strongly influence CA2 activity (Chevaleyre and Siegelbaum, 2010), we next aimed to test whether the exposure to HFD also altered transmission at these synapses. Upon stimulation of EC afferents to CA2 in hippocampal slices, we observed that the amplitude of the PSP was significantly larger in HFD-fed mice (Fig 1J**,** CD: n=22,13; HFD: n=27,10; p= 0.0012 for diet effect of stimulation 1; p=0.099 for diet effect of stimulation 2). We saw no difference in inhibitory transmission with a stimulation pipette placed in the stratum lacunosum moleculare (slm) (Sup Fig 3A, CD: n=8,6; HFD: n=5,4; p= 0.087 for diet effect of stimulation 1 without blockers of excitatory transmission; p= 0.093 for diet effect of stimulation 1 with blockers of excitatory transmission). However, we did detect a reduction in inhibitory current amplitude on the second pulse (p=1.2E-5 for diet effect of stimulation 2

without blockers of excitatory transmission; p=1.6E-5 for diet effect of stimulation 2 with blockers of excitatory transmission). Like what we observed at the CA3-CA2 synapse, we also detected a significant decrease in the PPR of inhibitory transmission when distal inhibitory inputs were directly stimulated (Sup Fig 3B, CD: n=8,6; HFD: n=5,4; p= 0.048 for diet effect), possibly indicating a change in the inhibitory transmission onto area CA2 in this dendritic compartment.

It has been reported that a single week of HFD exposure can have effects on hippocampal function (Khazen et al., 2019). Therefore, we examined synaptic transmission at different timepoints following exposure to HFD. We fed mice with a HFD or CD for 10 days or 5 weeks and compared the amplitude of the recorded CA3-CA2 field PSPs normalized by fiber volley amplitude. 10 days or 5 weeks of a HFD was not sufficient to increase SC to CA2 transmission (Sup Fig 4A-C, 10 days: CD: n=12,4; HFD: n=12,4, p=0.071; 5-weeks: CD: n=23,6; HFD: n=31,8, p=0.83). As HFD did not affect weight gain after 10 days or 5 weeks (Supp Fig 1B), this suggests HFD effect on CA2 excitability may require morphometric and metabolic changes as evidenced after 12 weeks of HFD exposure (Supp Fig 1B-C).

HFD exposure does not alter CA2 PN intrinsic properties

To better understand the effect of HFD-exposure on CA2 PN physiology, we examined the intrinsic properties of the cells in both HFD-fed and CD-fed mice. HFD exposure did not affect CA2 PN resting membrane potential, membrane resistance, membrane capacitance, sag, rheobase current nor AP threshold (Sup Fig 5A-F). For a set injected current, CA2 PNs of HFD-fed mice fired APs similar to CD-fed CA2 PNs (Sup Fig 5G). Nevertheless, we observed that a HFD modified the AP shape of CA2 PNs upon current injection. Indeed, although rise time, amplitude and after-hyperpolarization of CA2 PN APs were unaltered, a HFD reduced the half-width and the decay-time constant of CA2 PN APs (Sup Fig 6A-F, CD: n=49,36; HFD: n=54,35; p=0.020 for AP half-width; p=0.035 for AP decay time-constant).

Inhibition of dCA2 PNs rescues SRM deficits in HFD-fed mice

We postulated that the compromised SRM we observed may be due to the increased synaptic transmission of dCA2 following exposure to a HFD, even though the intrinsic properties and synaptic plasticity were not altered. To test this hypothesis, we injected an AAV vector expressing floxed-hM4D(Gi) DREADDs or a control vector expressing floxed-mCherry bilaterally in the dCA2 area of *Cacng5*-Cre mice to selectively inhibit CA2 PN activity following CNO administration (Fig 2A-B). After habituation to a test environment, CNO was

administered in both CD and HFD-fed mice before a training trial when the mouse is presented a novel conspecific. We found that sociability was unaltered by virus expression or diet (Fig 2C-D, $p<0.001$ comparison with 50% or 0 in the sociability index). The social discrimination test 3 hours later showed that CNO injection in the HFD-fed mice expressing hM4D(Gi) mice was sufficient to rescue SRM deficits (Fig 2E-F, HFD Gi: $n=11$, $p<0.001$). Transient inhibition of CA2 PNs in CD-fed mice impaired SRM (Fig 2E-F, CD Gi: $n=8$, $p>0.05$). Interestingly, CA2 inactivation did not affect social recognition when the mice were discriminating between a novel mouse or a familiar cage mate, as all groups investigated the novel mouse, indicating an effect of CA2 manipulation on novel social memory formation rather than on social discrimination *per se* (Fig 2 G-J). Moreover, inhibition of CA2 PNs did not rescue HFD-induced deficits in object recognition memory (Fig 2J-L), a task that does not require area CA2 (Hitti and Siegelbaum, 2014).

HFD exposure results in disrupted oxytocin receptor signaling in area CA2

Following exposure to a HFD, a reduction in hippocampal OT signaling has been reported (Hayashi et al., 2020; Khazen et al., 2022). According to the role of OT in prosocial behavior, we decided to examine this further. We measured OTR expression in HFD-fed or CD-fed mice in hippocampal areas CA1, CA2 and the dentate gyrus at baseline (home cage) or following a novel social interaction. In area CA1, there was a significant effect of diet on OTR gene expression with lower expression in HFD-fed mice for both the novel social and control conditions (Fig 3A). Interestingly, in area CA2 there was a significant interaction between diet and condition. We detected a significant increase in OTR gene expression in CD-fed mice that had encountered a novel conspecific as compared to home-cage controls and to HFD-fed mice that had social interaction. In HFD-fed mice, however, there was no significant difference in the OTR gene expression in mice that had novel social interaction as compared to home-cage controls (Fig 3A). For the dentate gyrus, we detected no effect of diet, social interaction or interaction on OTR gene expression.

Exposure to HFD has previously been shown to alter the dendritic morphology of CA1 PNs and dentate gyrus granule cells (Sarfert et al., 2019). To examine how CA2 dendritic morphology is altered following HFD-exposure, we reconstructed the dendritic arbors of CA2 PNs that had been biocytin-filled during whole-cell recording (Fig 3B). We performed sholl analysis and found a significant reduction in the number of intersections of basal, but not apical dendrites in HFD-exposed animals as compared to control (Fig 3C). Although the total

length of apical and basal dendrites were similar in both groups, quantification of the dendritic nodes and dendritic order number revealed significant reductions for basal dendrites in the HFD-exposed mice as compared to CD (Fig 3D). These results are similar to reports of dendritic morphology changes of CA2 PNs in OTR knock-out mice (Lin et al., 2018). Thus, we hypothesize that perhaps OT signaling in area CA2 may be disrupted in HFD-exposed animals.

OTR activation is known to have two major effects on the physiology of CA2 PNs. Activation of OTRs by selective agonist application in slices results in CA2 PN membrane depolarization and spontaneous bursting activity (Tirko et al., 2018; Liu et al., 2022). Additionally, OTR activation in slices has been shown to result in the potentiation of glutamatergic transmission at the CA3-CA2 and EC-CA2 synapses, as well as a depression of inhibitory transmission recruited by perforant path stimulation (Pagani et al., 2014; Lin et al., 2018). To examine this further, we tested whether HFD exposure altered OT-induced CA2 PN depolarization and bursting using whole-cell recordings of CA2 PNs following 1 μM OT application. Application of OT induced burst firing in CA2 PNs in both CD and HFD fed groups (Fig 3E-F, CD: 40%, n=20,10; HFD: 64.7%, n=17,9; p=0.13). Furthermore, the membrane depolarization preceding bursting activity was significantly higher in HFD-fed mice as compared to CD-fed littermates (Fig 3G-H, CD: n=17,9, 7.56±0.70mV; HFD: n=16,78, 10.56±0.86mV; p=0.018). For all the CA2 PNs that had bursting activity, HFD exposure did not significantly alter burst onset, duration, number of bursts, number of APs per burst, firing rate during the bursts or the inter-burst interval (Sup Fig 7).

We then examined whether HFD exposure altered the ability of OTR activation to enhance CA2 PN intrinsic excitability. To do this, we examined the number of APs elicited with current injection as well as the intrinsic properties of CA2 PNs before and during OT application. As expected, OT application caused a leftward shift in the AP number per current injected in both CD and HFD groups (Sup Fig 8A-B). OT also induced a decrease in rheobase current, an increase in membrane resistance and an increase in and sag in both CD and HFD groups (Sup Fig 8C-F). Interestingly, while OT increased AP threshold of CA2 PNs in the CD-fed mice, this did not occur in the HFD-fed mice (Sup Fig 8E). As previously reported (Tirko et al., 2018), activation of OTRs results in a change in the AP shape in CA2 PNs. In our results, AP half-width and AP decay time constants were reduced by OT application in both diet groups (Sup Fig 9A-D). Because AP half-width and decay time constants were already reduced at baseline in HFD-fed mice, these measures were also lower in HFD-fed

mice compared to CD-fed mice upon OT application (Sup Fig 9D-E). While this small OT-induced increase in AP decay time may potentially result in more calcium entry per individual AP, and hence, increased global excitability of CA2 PNs, the change is relatively small compared to the large increase in synaptic transmission in area CA2 following HFD exposure. Thus, while some aspects of OT-induced enhanced intrinsic excitability are altered in HFD conditions, we doubt that these alone are sufficient to account for the large effect of HFD on SRM.

A HFD impairs OT-mediated long-term potentiation of CA3-CA2 synapses

Activation of OTRs in area CA2 is known to result in a long-term increase in synaptic transmission at the CA3-CA2 synapse (Pagani et al., 2014). To determine if HFD-exposure impaired potentiation of CA3-CA2 responses, we measured the change in synaptic transmission following application of 1 µM OT while maintaining the cells at -70 mV in current-clamp mode. In slices prepared from HFD-fed mice, application of OT resulted in reduced potentiation of CA3-CA2 synapses as compared to CD-fed mice (Fig 4A-B, CD: n=15,13 p=1.0E-4 baseline vs 40-50min; HFD: n=15,12 p=0.0023 baseline vs 40-50min; CD vs HFD: p=0.0081). To better understand the synaptic mechanisms of this change, we tested whether a HFD altered OT-induced changes in inhibitory transmission by recording cells in voltage clamp mode at +10 mV to isolate IPSCs and blocked all excitatory transmission with AMPAR and NMDAR blockers (AP-5 and NBQX). OT application led to a long-term depression of IPSCs onto CA2 PNs, as had previously been reported (Lin et al., 2018) upon stimulation of the perforant path input to CA2 for both HFD and CD-fed mice (Fig 4C-D, CD: n=7,5 p=0.0049 baseline vs 30-40min; HFD: n=8,6, p=0.0041 baseline vs 30-40min; CD vs HFD: p= 0.63). These results suggest that HFD exposure does not alter the effect of OTR activation on inhibitory transmission in area CA2. We performed extracellular recordings of excitatory transmission onto area CA2 in the presence of GABAR blockers and confirmed that 1µM OT application induced a smaller potentiation of transmission in HFD-fed mice as compared to the potentiation induced in their CD-fed siblings (Fig 4E-F, CD: n=13,7, p=2.0E-5 baseline vs end; HFD: n=13,9, p=2.4E-4 baseline vs end; CD vs HFD: p= 0.021).

Because we saw that HFD exposure resulted in increased excitatory transmission at the CA3-CA2 synapse (see Fig 1F-I), we postulated that perhaps the reduced potentiation following 1 µM OT application may be due to an occlusion, or ceiling effect of the OT-dependent potentiation in HFD-fed mice. We tested whether electrical stimulation led to higher OT

release in slices of HFD-fed mice compared to CD-fed mice. Antagonizing OTRs via application of 1µM of L-37 did not alter excitatory transmission onto CA2 PNs in HFD or CD-fed mice (Sup Fig 10), suggesting that no basal OT is released with electrical stimulation in hippocampal slices in area CA2 in our experiments.

To test whether the impairment in OT-induced LTP in HFD-fed mice can be rescued via application of a higher concentration of OT, we applied 10µM of OT. This high OT concentration rescued the potentiation in HFD-fed mice back to CD-fed levels (Fig 4G-H, CD: n=12,5, p=0.0026 baseline vs end; HFD: n=9,5, p=0.017 baseline vs end; CD vs HFD: p= 0.67), suggesting that HFD-fed mice do express functional OTRs and downstream pathways leading to plasticity in CA2 PNs, but that the OTRs in HFD-exposed mice may be less sensitive to OT or less efficient.

Application of 1µM OT is permissive for eCB-mediated plasticity in area CA2 in CD but not HFD-fed mice

It has previously been demonstrated that expression of OTRs in CA2/CA3a PNs is necessary for SRM (Raam et al., 2017; Lin et al., 2018; Tsai et al., 2022). Furthermore, it has also been shown that synaptic plasticity of inhibitory synapses is required for SRM (Loisy et al., 2022). To better understand the changes occurring in HFD-fed mice, we examined both the DOR-mediated and eCB-mediated long-term depression of inhibitory transmission (iLTD) in area CA2. These synaptic plasticities occur on separate population of inhibitory terminals. Furthermore, the eCB-mediated iLTD in area CA2 requires the PN to fire action potentials, causing calcium influx and eCB release (Sup Fig 11A-B). The DOR-mediated iLTD has been shown to be permissive, as it reduces inhibitory transmission enough to allow CA2 PNs to fire APs. We found that exposure to HFD had no significant effect on the DOR-mediated LTD at inhibitory terminals in area CA2, as examined by input stimulation (Sup Fig 11C). HFD exposure also had no effect on eCB-mediated iLTD, as tested by ACEA application (Sup fig 11D), direct depolarization of the post-synaptic CA2 PN to fire APs (Sup Fig 11E) and input stimulation following DOR iLTD induction (Sup Fig 11F).

Activation of OTR leads to membrane depolarization and AP firing, and this likely leads to eCB release. To test this potential mechanistic link between OTR activation and eCB iLTD, we decided to examine if 1 µM OT application could be permissive for eCB-mediated plasticity. To do this, we used a sub-threshold tetanus induction protocol of two trains of 25 pulses at 10 Hz that induced a consistently small, ~20% increase in the field potential

amplitude in both CD and HFD conditions (Sup Fig 12). In CD-fed mice, we applied 1µM OT 5 minutes before applying the sub-threshold induction protocol. This chain of events effectively induced a strong increase in fPSP amplitude at CA3-CA2 synapses (Fig 5A-C, 39.23±5.38% increase, p=9.6E-5 baseline vs 50-60min, CD OT+tetanus: n=10,8) that was blocked by the CB1R inverse agonist AM251 (Fig 5C, 9.00±6.07% increase, p=0.16 for baseline vs 50-60min; OT+tetanus+AM251: n=8,7; p=0.0022 for difference between groups). Thus, this increase in fPSP is due to the eCB-mediated disinhibition of the CA3-CA2 synapse. We verified that the increase of fPSP amplitude was not due to the sub-threshold tetanus alone or OT application alone with interleaved control experiments. The largest increase in field potential occurred only with the combination of both OT application and subsequent sub-threshold tetanus (Fig 5D, p=0.024 for OT+tetanus versus OT only; p=0.0015 for OT+tetanus versus tetanus alone). Thus, a brief application of 1µM OT is therefore permissive for eCB plasticity induction in area CA2.

In HFD-exposed animals, no eCB-mediated increase in field potential was observed with the sub-threshold tetanus following 1 µM OT application (Fig 5E). We propose that compromised OT signaling may prevent the eCB-mediated plasticity from occurring in these conditions in HFD mice. In HFD-exposed mice, OT application followed by a subthreshold tetanus produced no additional increase in fPSP than the sub-threshold tetanus alone, or OT application alone (Fig 5F).

OTR activation results in depolarization and bursting of CA2 PNs (Fig 3E-H). It may be that this spontaneous activity may lead to eCB release by CA2 PNs. To examine this further, we verified that the potentiation of transmission at the CA3-CA2 synapse following OT application was not due to eCB-mediated disinhibitory plasticity by applying AM251. We found that under these conditions, there was no change in OT-induced potentiation of transmission (Sup Fig 13).

10 µM OT can rescue eCB-mediated plasticity in HFD-fed mice

Our results support the idea that OT signaling is disrupted in HFD-fed mice, as indicated by the reducedability 1 µM OT to induce LTP as well as absence of eCB-mediated plasticity following 1 µM of OT application. Because a higher concentration was able to rescue the OT-mediated LTP in HFD conditions (Fig 4G), we examined whether a higher concentration of OT could also recue the OT-induced eCB plasticity in HFD-fed mice. To test this, we used the same experimental paradigm with a 10 µM OT application before the sub-threshold tetanus

induction protocol. In CD conditions, we found that the resulting increase in field potential with both tetanus and 10 µM OT was the same as what we observed with application of 10 µM OT alone (Fig 6A-C).

Because a higher concentration of OT elicits strong CA2 PN bursts on its own, we tested whether the 10 µM OT application alone was sufficient to induce eCB-mediated plasticity in area CA2. We found that application of the CB1R inverse agonist AM251 impaired 10 µM OT-induced increase of CA3-CA2 fPSP amplitude (Fig 6D). We next examined how the coupling between 10µM OT and eCB-mediated plasticity was altered by HFD-exposure. In HFD-fed mice, application of 10 µM OT led to the same increase in fPSP amplitude with or without the sub-threshold tetanus **(**Fig 6E) and was sufficient to induce eCB plasticity in HFD-fed mice (Fig 6F, p=0.0051, HFD OT only vs HFD OT+AM251). Thus, these results indicate that both the OT-mediated LTP and the e-CB-mediated disinhibition are both potentially dysfunctional in HFD-fed mice, but can be rescued with higher OT application.

Injection of a high, but not low, concentration of OT in dCA2 rescues SRM deficits in HFD-fed mice

We have shown that in HFD-exposed mice, 10 µM OT is able to rescue in dCA2 both the OT-mediated potentiation as well as enable eCB-mediated disinhibitory increase in fPSPs. This is in contrast to 1 µM OT application. We hypothesized that an increased OT during social interaction may rescue the SRM deficits of HFD-fed mice. To test this, we bilaterally implanted cannulas in dCA2 (Fig 7A-B) and delivered either vehicle, 1 ng or 10 ng OT (corresponding to 5 µM and 50 µM OT, respectively) in 0.2 µL bilaterally 10 minutes prior to the training phase of the SRM test in both CD-fed and HFD-fed mice. Injection of vehicle or OT at both concentrations did not alter sociability either in the CD-fed or HFD-fed mice (Fig 7C-D). During the SRM testing, we observed that vehicle-infused CD-fed mice exhibited normal ability to discriminate between familiar and novel conspecifics. However, the CD-fed animals that received either the 5 µM or 50 µM OT injection displayed impaired SRM, as evidenced by their poor discrimination between the familiar and novel stimuli. In HFD-fed mice, those injected with vehicle displayed impaired SRM. Likewise, SRM performance was still impaired with 5 µM OT injection. In contrast, HFD-fed animals that received the 50 µM OT injection in dCA2 had rescued SRM (Fig 7E-F). These results indicate that exogenous OT injection in dCA2 in CD-fed animals during social interaction can effectively perturb

subsequent SRM performance. However, in the HFD-fed mice, the elevated OT is sufficient to rescue SRM deficits.

DISCUSSION

Two novel mechanisms of neuromodulation-induced plasticity in area CA2

Our results reveal a novel link between OT neuromodulation and eCB inhibitory plasticity in area CA2. It has been previously been shown that induction of a delta-opioid receptor-mediated disinhibitory plasticity allows for CA2 PN AP firing is permissive for eCB plasticity induction in area CA2 (Loisy et al., 2022). It was also demonstrated that the DOR-plasticity was very sensitive to environmental factors, and appeared to be occluded following 3 weeks of environmental enrichment (Loisy et al., 2023). Thus, the sequential mechanism linking these two plasticities seems unlikely if the DOR-mediated plasticity only occurs in sub-standard environemnts. Here, we demonstrate that OTR activation in area CA2 is permissive for eCB-mediated iLTD. This OT-induced eCB plasticity is likely a more relevant avenue to allow for eCB plasticity because OT release has critical importance for social memory formation *in vivo.* In another area receiving OT projections from the PVN, the NAc, OT release (via excitatory DREADD expression) has also been shown to drive eCB-mediated signaling (Wei et al., 2015). Here, we demonstrated that application of 1 µM OT prior to a sub-threshold induction protocol resulted in eCB iLTD. We demonstrate that in our preparation, this concentration of OT is sufficient to depolarize CA2 PNs and can lead to burst AP firing. This depolarization of CA2 PNs and AP firing is likely allowing for the sufficient intracellular calcium entry into CA2 PNs to enable eCB release (Loisy et al., 2022).

dCA2 hyperexcitability impairs SRM in HFD-fed mice

Although it does not seem that CA2 PN excitability *per se* is altered in HFD-fed mice, stimulation of intrahippocampal afferents from the EC and dorsal CA3 are aberrantly strong. Both of these inputs onto area CA2 have been reported to affect SRM (Lopez-Rojas et al., 2022; Pan et al., 2022). Here we showed that inhibition of CA2 PNs through chemogenetics during memory formation of a social encounter was sufficient to rescue SRM deficits in HFD-fed mice, while it impaired SRM in CD-fed counterparts. This result goes hand-in-hand with previously published reports showing that not only is CA2 activity necessary for SRM, but

that its activity must be finely tuned in order to engage in proper social memory formation (Pan et al., 2022).

Two distinct CA2 strategies to rescue HFD-induced SRM deficits

It is surprising that both chemogenetic inhibition of CA2 PNs and injections of a high dose of OT in area CA2 rescues SRM impairments in HFD-fed mice, as OT application increases excitability and spontaneous burst firing of CA2 PNs (Tirko et al., 2018). From recent work, we postulate that astrocyte signaling may be playing a role in this phenomenon. It has been demonstrated that astrocytes in several brain regions express astrocytes that contain OTRs (Wahis et al., 2021; Farsetti et al., 2025; Meinung et al., 2025). Furthermore, OTRs in astrocytes are linked to different G-protein coupled pathways that display difference concentration dependances on their activation (Farsetti et al., 2025). Thus, while we observe a link between eCB release and OTR activation in CD animals at low OT concentration, it is possible that exposure to HFD is having a detrimental effect on CA2 astrocyte OTR signaling. Thus, the higher concentration of OT is required to rescue SRM in HFD-fed animals, while not in CD animals.

Exogenous OT injection in dCA2 impairs SRM in CD-fed mice

It was surprising that both low and high OT injection in dCA2 impaired social discrimination in CD-fed mice. Indeed, it has been demonstrated that chemogenetic activation of OT afferents in dCA2 during the training phase enhanced SRM (Tsai et al., 2022). The exogenous nature and artificially high concentration of OT application could perhaps explain these contradicting findings. Indeed, previous report indicated that high levels of OT can trigger social amnesia (Popik and Vetulani, 1991; Popik et al., 1992; Zhan et al., 2024), revealing that an optimal OT level is required for SRM. Again, we suspect that astrocyte signalling may be affected in a concentration-dependant manner in the hippocampus and merits further investigation.

A HFD impairs low, but not high, concentration effects of OT signaling

It is notable that low, but not high, OT concentration are ineffective to induce potentiation of transmission at the CA3-CA2 and EC-CA2 synapses as well as eCB-mediated iLTD in area CA2 in HFD-fed mice. It is not so clear if these two results are linked as the mechanism of action leading up to eCB release requires high intracellular calcium concentrations from AP firing. It would be more probable that enhancement of CA2 PN excitability is what allows

eCB plasticity in area CA2, yet this OT-dependent effect is not affected in HFD-fed mice. We suggest that, in these mice, the shortening of APs underneath a certain threshold following OT application impairs sufficient calcium entry eventually impeding the eCB plasticity. Because OT induces stronger depolarization and bursting in higher proportions in HFD-fed mice, high dose of OT (without electrical stimulation) may allow for eCB plasticity in HFD-fed mice through this compensation.

A link between hyperexcitability and OT signaling impairments in HFD-fed mice

The lack of OT-induced plasticity of the CA3-CA2 synapse in HFD-fed mice may decrease CA2 excitability in some contexts: this dysregulation might have led to a homeostatic compensatory increase in excitatory hippocampal inputs onto CA2. Indeed, it seems that the hyperexcitability phenotype observed in HFD-fed mice takes a long time to develop (as 10 days or 5 weeks of a HFD does not entail larger transmission at the CA3-CA2 synapse for a set number of stimulated axons) which could be the result of a delayed adaptation. Nevertheless, even if the hyperexcitability of area CA2 is an adaptation to a lack of OT-induced effect, it seems to be a maladaptive one as it perturbs effective encoding and adds noise to hippocampal information transfer.

Are there OT release deficits in HFD-fed mice *in vivo?*

As OT release in the PVN has been reported to be reduced as a consequence of a HFD (Zhang and Cai, 2011; Wu et al., 2017), we can imagine that PVN OT release in dCA2 may be altered as well. Furthermore, the enhanced depolarization of CA2 PNs upon OT application in HFD conditions could be a resulting compensation due to lower OT signaling after social interactions. Studying the PVN-CA2 OT projections and using optogenetic stimulation of PVN OT afferents onto dCA2 area could help us further elucidate what the underlying causes of OT-dependent signaling impairments in area CA2 are. Regardless, even upon application of exogenous OT, a HFD impairs OT-dependent signaling. Although this may be a result of altered release onto the dCA2 area *in vivo*, this highlights the fact that the consequence of OT release in CA2 (even if adequate) is malfunctioning under HFD condition. Alternatively, it has been demonstrated that the supramammillary nucleus (SuM) expresses OTRs, and that the CA2-projecting cells in the SuM are playing an important role in SRM (Chen et al., 2020; Thirtamara Rajamani et al., 2024). Thus, it may be that the injection of OT may be acting more on the pre-synaptic SuM inputs for the rescue of social memory. This merits further exploration.

AUTHOR CONTRIBUTIONS

Conceptualization: MM, AF, ED, VC, RAP and GF. Investigation: MM, AF, ED, VC. Analysis: MM, AF, ED, VC, RAP. Writing: MM and RAP.

ACKNOWLEDGMENTS

The authors thank the animal facility team of NutriNeuro lab, particularly Gregory Artaxet, for taking daily care of the animals. This work was supported by Fondation pour la Recherche Médicale EQU202003010457 to VC and RAP and French National Research Agency (ANR-18-CE370020-01, ANR-18-CE16-0006 and ANR-21-CE16-0021-03 to VC and RAP and ANR-23-CE14-0004 HIPPOBESE to GF, VC and RAP). MM was the recipient of a PhD fellowship from the French Ministry of Research and Higher Education (2020-2023). AF was the recipient of a PhD fellowship (2020-2023) from the Bordeaux NeuroCampus Graduate Program, managed by the French National Research Agency (ANR-17-EURE-0028), and an extension grant from the French government in the framework of the University of Bordeaux's France 2030 program / GPR BRAIN_2030 (2023-2024).

FIGURE LEGENDS

Figure 1. A 12-week HFD impairs social recognition memory and enhances area CA2 excitability upon SC stimulation can be rescued by CA2 PN inhibition

A. Behavioral Paradigm. **B-C.** Both CD-fed and HFD-fed mice preferred the social target as reflected by the percentage of time spent exploring the social stimulus compared to the non-social stimulus (CD: n = 16, HFD: n = 15, $p < 0.001$ compared to 50%) as well as the sociability index (CD: n = 13, HFD: n = 14, $p < 0.001$ compared to 0). **D.** After a 15-minute delay, both CD-fed and HFD-fed mice spent significantly more time exploring the novel mouse compared to the familiar one (CD: n = 15, HFD: n = 10, $p < 0.05$ compared to 50%). After a 3-hour delay, CD-fed mice still spent significantly more time exploring the novel mouse than the familiar one (CD: n = 16, $p < 0.01$), whereas HFD-fed mice spent equal amounts of time exploring both the novel and familiar mice (HFD: n = 15, $p > 0.05$) leading to significant group difference (CD: n = 16, HFD: n = 15, $p < 0.05$). **E.** The discrimination index was significantly greater than 0 in both CD-fed and HFD-fed mice after a 15-minute

delay (CD: n = 15, HFD: n = 10, $p < 0.05$). After a 3-hour delay, the discrimination index remained significantly greater than 0 for CD-fed mice (CD: n = 16, $p < 0.01$) but not for HFD-fed mice (HFD: n = 15, $p > 0.05$), with an index significantly higher in CD-fed mice compared to HFD-fed mice ($p < 0.05$). **F**. Left: Schematic of recording configuration. Middle: Example traces of CA2 fPSPs upon SC stimulation for HFD and CD-fed mice. Right: fPSP vs FV graph for HFD and CD-fed mice at 10, 20 and 30V stimulation intensities; far right, HFD increases fPSP normalized on FV per stimulation intensity in CA2 upon SC stimulation (HFD: n=23,10, CD: n=13,6; p=0.016 for diet effect.). **G**. Left: schematic of whole-cell recording configuration. Middle: example traces of PSPs recorded in HFD and CD-fed mice. Right: A HFD increases PSP amplitudes for a set stimulation intensity in CA2 PNs upon SC stimulation (HFD: n=34,18; CD: n=23,17; p=0.0052 for diet effect stimulation 1; p= 0.014 for diet effect stimulation 2). **H.** Left: schematic of recording conditions. Middle: example EPSP traces in CA2 PNs upon SC stimulation. Right: A HFD increases EPSP amplitudes in CA2 PNs upon SC stimulation (CD: n=9,4; HFD: n=8,3; p=0.0064 for diet effect stimulation 1; p= 0.014 for diet effect stimulation 2); far right, a HFD decreases excitatory transmission paired-pulse ratio (CD: n=9,4; HFD: n=8,3; p=0.0041 for diet effect.). **I.** Left: schematic of recording configuration. Middle: example population spike (PS) traces in CA2 upon SC stimulation. Right: A HFD enhances population spike amplitude upon SC stimulation (CD: n=18,7; HFD: n=23,6; stimulation 1: 10V p=0.59; 20V: p=0.32; 30V: p=0.0089; stimulation 2: 10V: p=0.072; 20V: p=0.0023; 30V: p=0.0039). **J**. Left: Schematic of recording conditions. Middle: example traces of transmission onto CA2 PNs upon PP stimulation. Right: A HFD increases PSP amplitude in CA2 PNs upon PP stimulation (CD: n=22,13; HFD: n=27,10; p= 0.0012 for diet effect of stimulation 1; p=0.099 for diet effect of stimulation 2).

Figure 2. HFD-induced social memory deficits can be rescued by CA2 PN inhibition. **A.** Behavioral paradigm of AAV-mediated Gi-DREADD expression in CA2 PNs for SRM testing**. B.** Example confocal image of AAV virus-mediated delivery of vectors in dCA2. Scale bar is 200 µm. **C**. HFD and CD mice, injected with either mCherry control virus or Gi-DREADD virus, explore the social stimulus a greater amount of time compared to the non-social one ($p<0.001$ for comparison between time exploring social and non-social stimulus in all groups). **D.** Sociability index for social versus non-social stimuli is different than 0 in both CD and HFD-fed mice ($p<0.001$ for comparison with 0). **E.** In the test phase, CD-mCh mice explore the novel mouse a greater amount of time compared to the familiar one ($p<0.01$ for comparing time of exploration between familiar and novel mouse). CD-Gi and HFD-mCh

mice explore the novel and familiar mice the same amount of time ($p>0.05$). HFD-Gi mice explore the novel mouse a greater amount of time compared to the familiar one ($p<0.01$). Percentage time exploring the novel mouse is greater in CD-mCh and HFD-Gi vs HFD-mCh ($p<0.05$ for both comparisons). **F.** Discrimination index is higher than 0 in CD-mCh and HFD-Gi ($p<0.01$ and $p<0.001$ respectively), but not in CD-Gi or HFD-mCh mice($p>0.05$). **G.** Behavioral paradigm of AAV-mediated Gi-DREADD expression in CA2 PNs for SRM testing between a cagemate and novel conspecific. **H.** HFD and CD mice, injected with either mCherry control virus or Gi-DREADD virus, explore the novel mouse a greater amount of time compared to the cagemate ($p<0.05$ for CD-mCh, $p<0.005$ for CD-Gi and HFD-mCh, and $p<0.01$ for HFD-Gi comparison between time exploring novel and cagemate in all groups). **I.** Discrimination index is higher than 0 for all conditions. **J.** Behavioral paradigm of AAV-mediated Gi-DREADD expression in CA2 PNs for novel object discrimination testing. **K.** No significant difference in exploration time of identical objects in different locations was observed for all conditions. **L.** In the test phase, the CD-nCh ($p < 0.05$) and CD-Gi ($p < 0.01$) mice showed increase exploration of the novel object, whereas the HFD-fed animals did not show significant exploration times of the novel and familiar object. The number of animals used per group is shown on the figure.

Figure 3. A HFD reduces basal dendrite complexity of CA2 PNs. **A.** OTR gene expression, as detected by qPCR, in areas CA1, CA2 and dentate gyrus in mice 60 minutes following exposure to either a novel mouse for 10 minutes (social) or their home cage (ctl) for both CD and HFD conditions. **B**. Example reconstructions of CA2 PNs of CD (top) and HFD (bottom, blue) fed mice. **C.** Sholl analysis of basal (top) and apical (bottom) dendrites for HFD (blue) and CD (black) CA2 PNs (basal : CD: n=17,10; HFD: n=20,13) (apical : CD: n=17,10; HFD: n=20,13). **D.** Top left, total basal dendritic length for CD and HFD CA2 PNs (CD: n=17,10; HFD: n=20,13; p=0.46). Top center, number of basal branches for CD and HFD CA2 PNs (CD: n=17,10; HFD: n=20,13; p=0.036) Top right, number of orders of basal dendrites for CD and HFD CA2 PNs (CD: n=17,10; HFD: n=20,13; p=0.044). Bottom left, total apical dendritic length for CD and HFD CA2 PNs (CD: n=17,10; HFD: n=20,13; p=0.12). Bottom center, number of apical branches for CD and HFD CA2 PNs (CD: n=17,10; HFD: n=20,13; p=0.39). Bottom right, number of orders of apical dendrites for CD and HFD CA2 PNs (CD: n=17,10; HFD: n=20,13; p=0.60). Filled circles represent CA2 PNs from male mice; empty circles represent CA2 PNs from female mice. **E.** Example traces of OT-induced CA2 PN bursting for CA2 PNs from CD and HFD fed mice. **F.** Top**,** 8 of 20 (40%) of CA2 PNs of

CD-fed mice burst upon 1µM OT application. Bottom: 11 of 17 (64.7%) of CA2 PNs of HFD-fed mice burst upon 1µM OT application (CD: n=20,9; HFD: n=17,8; p=0.13). **G.** Average depolarization of CA2 PN upon 1µM OT application. **H.** OT-induced depolarization 5-minutes after application onset is stronger in CA2 PNs of HFD compared to CD-fed mice (CD: n=17,9, 7.56±0.72mV; HFD: n=16,7, 10.56±0.86mV; p=0.018).

Figure 4. A HFD impairs OT-induced long-term potentiation of CA3-CA2 responses in a concentration-dependent manner. A. Left: Schematic of whole-cell PSP recording of CA2 PN upon SC stimulation. Middle: 5-minutes 1µM OT application induces a stronger long-term increase in PSP amplitude in CA2 PNs in CD versus HFD-fed mice. Right: Example traces of 1µM OT-induced CA2 PSP responses in CD and HFD-fed mice. **B.** Percentage of 1µM OT-induced PSP potentiation for each recorded CA2 PN (measured at 10 last minutes of recording normalized to baseline) (CD: n=15,13 p=1.0E-4 baseline vs end; HFD: n=15,12 p=0.0023 baseline vs end; CD vs HFD: p=0.0081). **C.** Left: Schematic of whole-cell recording of CA2 PN upon stimulation in SR, in the presence of excitatory transmission blockers. CA2 PNs were held at +10mV in voltage-clamp. Middle: 5-minutes 1µM OT application induces a long-term decrease in IPSC amplitude in CD and HFD-fed mice CA2 PNs **D.** Percentage of 1µM OT-induced IPSC depression for each CA2 PN (measured at 10 last minutes of recording normalized to baseline) (CD: n=7,5 p=0.0049 baseline vs end; HFD: n=8,6, p=0.0041 baseline vs end; CD vs HFD: p= 0.63). **E.** Left: Schematic of field EPSP recording of CA2 PN upon SC stimulation in the presence of blockers of inhibitory transmission. Middle: 5-minutes 1µM OT application induces a stronger long-term increase in CA3-CA2 fEPSP amplitude in CD compared to HFD-fed mice. Right: Example traces of 1µM OT-induced CA2 fEPSP responses in CD and HFD-fed mice. **F.** Percentage of 1µM OT-induced fEPSP potentiation for each slice recording (measured at 10 last minutes of recording normalized to baseline) (CD:§§§q n=13,7, p=2.0E-5 baseline vs end; HFD: n=13,9, p=2.4E-4 baseline vs end; CD vs HFD: p= 0.021). **G.** Left: Schematic of whole-cell PSP recording of CA2 PN upon SC stimulation. Middle: 5-minutes 10µM OT application induces a long-term increase in PSP amplitude in CD and HFD-fed mice CA2 PNs. Right: Example traces of 10µM OT-induced CA2 PSP responses in both CD and HFD-fed mice. **H.** Percentage of 10µM OT-induced PSP potentiation for each recorded CA2 PN (measured at 10 last minutes of recording normalized to baseline) (CD: n=12,5, p=0.0026 baseline vs end; HFD: n=9,5, p=0.017 baseline vs end; CD vs HFD: p= 0.67). Filled circles represent CA2 PNs from male mice; empty circles represent CA2 PNs from female mice.

Figure 5. OT is permissive for eCB plasticity In CA2 of CD but not HFD-fed mice. A. Schematic of CA2 fPSP recording with SC stimulation. **B.** Experimental protocols to test for OT-induced eCB plasticity. **C.** 5-minute application of 1µM OT 10 minutes before an induction protocol (2*25 @10 Hz, 20V) allows for CB1R-dependent fPSP potentiation. Middle: example traces of fPSPs before and after induction protocol with and without AM251 (CB1R antagonist). Right: 5-minute application of OT + induction allows for long-term potentiation of fPSPs (p=9.6E-5 for difference with baseline). This effect is blocked if AM251 is applied (p= 0.16 for OT+AM251 difference with baseline; p=0.0022 for difference between groups; OT+10 Hz: n=10,8: OT+10 Hz+AM251: n=8,7). **D.** OT+10 Hz protocol allows for stronger fPSP potentiation than OT alone or induction alone in CD mice. Middle: example traces of fPSPs before and after induction protocol for the three conditions. Right: 5-minute application of OT+10 Hz allows for stronger long-term potentiation of fPSPs than OT alone or 10 Hz induction alone (p=7.8E-4 for OT alone difference with baseline; p=0.0011 for 10 Hz alone difference with baseline; p=0.024 for OT+10 Hz versus OT only; p=0.0015 for OT+10 Hz versus 10 Hz alone; OT+10 Hz: n=10,8: OT only: n=16,12; 10 Hz only: n=17,16;). **E.** 5-minute application of 1µM OT 10 minutes before an induction protocol (2*25 @10 Hz, 20V) allows for fPSP potentiation in CD but not HFD-fed mice. Middle: example traces of fPSPs before and after induction protocol in CD and HFD-fed mice. Right: 5-minute application of OT + induction allows for long-term potentiation of fPSPs in CD-fed mice, but not in HFD-fed mice (p= 0.030 for difference between groups; p= 0.065 for HFD OT+10 Hz for difference with baseline; CD OT+10 Hz: n=10,8: HFD OT+10 Hz: n=9,7). **F**. OT+10 Hz, OT only and 10 Hz only protocols allow for the same extent of fPSP potentiation in HFD mice. Middle: example traces of fPSPs before and after induction protocol for the three conditions. Right: 5-minute application of OT+10 Hz allows for similar long-term potentiation of fPSPs in three conditions (p= 0.13 for HFD OT alone difference with baseline; p= 2.8E-4 HFD 10 Hz alone difference with baseline; p=0.80 for OT+10 Hz versus OT only; p=0.20 for OT+10 Hz versus 10 Hz alone; HFD OT+10 Hz: n=9,7: OT only: n=14,10; 10 Hz only: n=15,14). All experiments were done in the presence of naltrindole.

Figure 6. A high concentration of OT allows for eCB-mediated plasticity in CA2 in CD and HFD-fed mice. Schematic of CA2 fPSP recording upon SC stimulation. **B.** Experimental protocols to test for OT-induced eCB plasticity. **C.** 5-minute application of 10µM OT 10 minutes before an induction protocol (2*25 @10 Hz, 20V) elicits long-term increase in the fPSP to the same extent as 10µM OT application alone in CD-fed mice. 10 Hz induction alone

does not result in an increase in the amplitude of fPSPs (44.60±5.99%, p= 3.4E-4 for OT+10 Hz baseline vs 50-60min; 45.52±7.93%, p=4.4E-6 for OT alone baseline vs 50-60min; 14.63±9.28%, p= 0.16 for 10 Hz alone baseline vs 50-60min). Middle: example traces of fPSPs before and after induction protocol. Right: 5-minute application of 10µM OT + 10 Hz and of 10µM OT alone allows for larger increase in potential than 10 Hz alone (p= 0.023 for OT alone vs 10 Hz alone; p=0.018 for OT+10 Hz vs 10 Hz alone; p=0.93 for OT alone vs OT+10 Hz; OT+10 Hz: n=7,5: OT alone: n=10,7; 10 Hz alone: n=7,5). **D.** Left: AM251 hinders 10µM OT-induced increase in the field potential by preventing eCB iLTD in CD-fed mice (OT only: 39.06±6.26%; p= 2.4E-4 baseline vs 50-60min; OT+AM251: 17.37±5.31%; p=0.010 for baseline vs 50-60min; OT only: n=10,7; OT+AM251: n=9,6). Middle: example traces before and after OT application with and without AM251 application. Right: Percentage of 10µM-OT induced fPSP potentiation is reduced when blocking CB1Rs (p=0.018 OT only vs OT+AM251). **E.** 5-minute application of 10µM OT 10 minutes before an induction protocol (2*25 @10 Hz, 20V) elicits long-term increase in the field potential that is the same magnitude as 10µM OT application alone in HFD-fed mice. 10 Hz induction alone elicits a smaller increase in potential of fPSPs (41.17±6.51%, p=0.022 for HFD OT+10 Hz baseline vs 50-60min; 45.82±6.22%, p=2.4E-5 for HFD OT alone baseline vs 50-60min; 16.94±7.35%, p= 0.032 for HFD 10 Hz alone baseline vs 50-60min). Middle: example traces of fPSPs before and after induction protocol. Right: 5-minute application of 10µM OT + 10 Hz and of 10µM OT alone allows for stronger increase in field potential than 10 Hz alone in HFD-fed mice (p= 0.0074 for HFD OT alone vs HFD 10 Hz alone; p=0.056 for HFD OT+10 Hz vs HFD 10 Hz alone; p=0.78 for HFD OT alone vs HFD OT+10 Hz; HFD OT+10 Hz: n=7,6: HFD OT alone: n=11,7; HFD 10 Hz alone: n=9,7). **F.** Left: AM251 hinders 10µM OT-induced increase of CA2 fPSP amplitude in HFD-fed mice (HFD OT only: 37.96±5.62%; p= 4.8E-4 baseline vs 50-60min; HFD OT+AM251: 12.72±4.99%; p=0.043 for baseline vs 50-60min; HFD OT only: n=11,7; HFD OT+AM251: n=8,4). Middle: example traces before and after OT application with and without AM251 application. Right: % 10µM-OT induced fPSP potentiation is reduced when blocking CB1Rs in HFD-fed mice (p=0.0051 HFD OT only vs HFD OT+AM251). All experiments were done in the presence of naltrindole.

Figure 7. High, but not low, concentration of OT injected bilaterally in dCA2 rescues SRM in HFD-fed mice, and both low and high OT injection in dCA2 impairs SRM in CD-fed mice. **A.** Behavioral paradigm**. B.** Example image of cannula implantations in dCA2. Scale bar corresponds to 100 µm. **C**. HFD and CD mice, injected either vehicle, low or high

concentration OT, explore the social stimulus a greater amount of time compared to the non-social one for comparison between time exploring social and non-social stimulus in all groups). **D.** Sociability index for social versus non-social stimuli is different than 0 in both CD and HFD-fed mice ($p<0.005$ for comparison with 0). **E.** In the test phase, CD vehicle mice explore the novel mouse a greater amount of time compared to the familiar one ($p<0.05$ for comparing time of exploration between familiar and novel mouse). CD-low OT and CD-high OT mice explore the novel and familiar mice the same amount of time ($p>0.05$). HFD-vehicle mice and HFD-low OT mice do not discriminate between the novel and the familiar mouse ($p>0.05$). HFD high-OT mice explore the novel mouse over the familiar mouse ($p<0.01$). **F.** Discrimination index is higher than 0 in CD-vehicle and HFD-high OT ($p<0.05$ and $p<0.01$ respectively), but not in CD-low OT, CD-high OT or HFD-vehicle and HFD-low OT mice ($p>0.05$). The number of animals used per group is shown on the figure.

STAR METHODS

Lead Contact and Material Availability

Further information and requests for resources and reagents should be directed to and will be fulfilled by the Lead Contact, Rebecca A Piskorowski (rebecca.piskorowski@sorbonne-universite.fr).

Experimental Model and Subject Details

Electrophysiology experiments:

All experiments were performed on Swiss male and female mice.

Behavioral experiments:

C57B6J male mice (Charles River, France) were used for behavioral experiments. They were housed in groups of five since weaning at P21 in standard breeding cages with food and water ad libitum, and were placed at a constant temperature (23 ± 1°C) under diurnal conditions (light-dark: 8:00AM–8:00PM). Mice were tested during the first half of the light period.

Immunohistochemistry:

Histology experiments were performed on wild type swiss or C57Bl/6J mice.

Declaration of Interests

The authors declare no competing interests.

Supplemental Items: Table S1 (statistical data)

Method Details

Animals and diet

Swiss male and female mice were housed in single-sex groups of two to five per cage where they had ad libitum access to food and water. The animal facility was temperature controlled (22°C), and maintained under a 12h light/dark cycle. All procedures were performed in accordance with institutional regulations (French Ministry of Research decision #12406–2016040417305913 v10). At weaning (3-weeks of age), litters were divided up by sex and into two-groups: one given a control diet and one a high-fat diet (HFD) in order to have age-matched, sex-matched sibling controls. The diets were given ad libitum for 12 weeks (and in some experiments, for 10 days or 5 weeks only) until the mice were euthanized and used for experiments. The HFD (D12451, Research Diet) consisted of 4.7 kcal/g. The control diet consisted of 2.9 kcal/g (A04, SAFE).

Hippocampal slice preparation

Animals were euthanized in accordance with institutional regulations under ketamine (20 mg/kg), xylazine (1.4 mg/kg) and isoflurane, and perfused transcardially with a modified sucrose cutting solution containing the following (in mM): Sucrose 110, NaCl 10, KCl 2.5, NaH2PO4 1.25, $NaHCO_3$ 30, HEPES 20, glucose 25, thiourea 2, Na-ascorbate 5, Na-Pyruvate 3, CaCl2 0.5, $MgCl_2$ 10. The hippocampi were rapidly harvested, placed in an Agar mold and cut into transverse 400 μm slices with a vibratome (Leica VT1200S, Germany) in the same sucrose cutting solution at 4°C. The slices were then transferred to an immersed-type chamber containing artificial cerebrospinal fluid (ACSF) at 32°C (in mM: 125 NaCl, 2.5 KCl, 10 glucose, 26 $NaHCO_3$, 1.25 NaH_2PO_4, 2 Na Pyruvate, 2 $CaCl_2$ and 1 $MgCl_2$) for approximately 15 minutes and then maintained at room temperature for at least 1.5 hours before recording. Cutting and recording solutions were both saturated with 95% O_2 and 5% CO_2.

Electrophysiological recordings

All electrophysiological experiments were performed in a recording chamber allowing perfusion with ACSF at 3 ml/min at 30°C. Data were obtained using a Multiclamp 700B

amplifier and digitized using a Digidata 1550. Data were sampled at 10 kHz. pClamp10 and Axograph software were used for data acquisition.

Field recordings

Extracellular field recordings of postsynaptic potentials (fPSPs) were recorded in current-clamp mode using a recording patch pipette (3-5 MΩ) containing 1 M NaCl and positioned in the middle of stratum radiatum in CA2. For measure of population spike (PS) activity, the recording electrode was placed in stratum pyramidale of CA2. In order to stimulate the Schaffer collateral (SC) pathway, a monopolar stimulating electrode (containing aCSF, and with a broken-off tip) was placed in stratum radiatum of CA1 in order to antidromically excite CA3-CA2 synapses. Synaptic potentials were evoked with a constant voltage stimulating unit (Digitimer Ltd.) set at 0.1 ms at a voltage range of 10–30 V.

Plasticity was induced with high-frequency stimulation (HFS; 100 pulses at 100 Hz repeated twice) in the case of delta opioid receptors-dependent plasticity induction, or 10 Hz stimulation (100 or 25 pulses at 10 Hz repeated twice, at 30 or 20V) in the case of eCB plasticity induction. When studying eCB plasticity without pre-incubation in DPDPE, an antagonist of delta-opioid receptors (Naltrindole) was bath-perfused during the induction in order to prevent delta opioid receptors-dependent plasticity.

Whole-cell recordings

All whole-cell recordings of CA2 pyramidal neurons (PNs) were performed “blind.” Area CA2 has extremely dense extracellular matrix, making visually guided recordings very challenging. A recording pipette with positive pressure was inserted deeply into the pyramidal cell layer parallel to stratum so that the tip of the recording pipette was even with the end of the mossy fibers. The pipette was then stepped deeper into the slice while a voltage step was delivered through the pipette. The amplitude of a 5-10 mV current step was monitored and used to determine when the pipette was close to a neuron, positive pressure was released, and a giga-ohm seal was formed.

Whole-cell recordings were performed with either a potassium or cesium-based intracellular solution depending on the experiment. The cesium-based solution contained the following (in mM): Cs- methyl sulfonate 135, KCl 5, EGTA-KOH 0.1, HEPES 10, NaCl 2, MgATP 5, Na_2GTP 0.4, Na_2-phosphocreatine 10 and had a pH of 7.2 and an osmolarity of 286–295 mOsm. The potassium based one contained (in mM): 135 potassium methyl-sulfate,

5 KCl, 0.1 EGTA-Na, 10 HEPES, 2 NaCl, 5 ATP, 0.4 GTP, Na_2-phosphocreatine 10 and had a pH of 7.2 and an osmolarity of 286–295 mOsm. The liquid junction potential was not corrected. The series resistance (typically 9-25 MΩ) was monitored throughout each experiment; cells showing a series resistance >25 MΩ or a change in series resistance > 15% were excluded from the analysis.

Post-synaptic potentials (PSPs) were recorded using K^+-internal solution in whole-cell current clamp mode with current injected to maintain V_{REST} at -70mV. Excitatory-PSPs (EPSPs) were obtained in the same configuration in the presence of $GABA_A$ and $GABA_B$ blockers. Inhibitory post-synaptic currents (IPSCs) were obtained in voltage-clamp mode at +10mV (reversal potential for glutamatergic transmission) using a Cs-internal solution. In order to obtain IPSCs free of feedforward inhibition, AMPAR and NMDAR blockers were applied in the bath.

Synaptic potentials and currents were evoked by stimulation with a patch pipette filled with aCSF and positioned in the middle of CA1 stratum radiatum or stratum lacunosum moleculare to stimulate SC or the perforant path, respectively. Like for field recordings, stimulation was evoked through a constant voltage stimulating unit (Digitimer Ltd.) set at 0.1 ms at a voltage range of 10–30 V.

In order to allow for eCB plasticity under whole-cell configuration which does not allow for CA2 PN action potential firing using electrical stimulation (due to feedforward inhibition, see (Chevaleyre and Siegelbaum, 2010)), short pulses of 1200pA at 100ms intervals were injected into the cell in voltage-clamp mode in order for the CA2 PN to fire. This was done via two trains of 25 7ms-long current injections. PSP and IPSC amplitudes were normalized to the baseline amplitude in plasticity experiments. The extent of long-term plasticity was estimated by using the mean response of each cell at 40-50 min after the induction protocol for whole-cell recordings, and at 50-60 min after the induction protocol for extracellular recordings and normalizing it to mean baseline response (10 minutes before induction).

Because recordings were performed blind, biocytin (HelloBio, 4 mg/mL) was added to internal solutions in order to confirm the identity of the recorded cell post-hoc via its position as well as its morphology (see section histology). In cells recorded from with K^+-based internal solution, electrophysiological properties of CA2 PNs were also used to confirm the identity of the cell (input resistance, membrane capacitance, resting membrane potential, and firing pattern) as described previously (Chevaleyre and Siegelbaum, 2010).

AP shape analysis

AP shape analysis was always performed on the first AP elicited at rheobase. Axograph was used to measured AP amplitude, 20-80% rise-time, half-width (the width of the AP at half of its maximum amplitude), decay time-constant (measured as the time of 67% AP decay) and after-hyperpolarization (measured as the minimal potential after each AP subtracted from the cell potential before AP firing) for each spike.

Burst analysis

Bursts were defined as groups of at least 2 action potentials firing at a frequency of more than 0.5Hz, lasting at least 1.5 seconds, and characterized by a slow rampant depolarization as well as an after-hyperpolarization (as is observed on the example shown in figure III.10). Bursting onset (measured as the time from drug application to first burst), Burst duration (measured as the duration of the depolarizing plateau phase of the burst), firing rate during bursts, number of APs per burst, inter-burst intervals and total number of bursts elicited (calculated withing 15 minutes of drug application) were measured via Axograph.

Pharmacology

Pharmacological agents were added to the ACSF at the concentrations reported in Table III.1.

Pharmacological agent	**Function**	**Concentration used in ACSF (µM)**	**Source**	**Identification**
CGP 55845 hydrobromide	$GABA_A$ receptor antagonist	2	Hello Bio	HB0960
SR 95531 hydrobromide	$GABA_B$ receptor antagonist	1	Tocris	1262
D-AP5	NMDA receptor antagonist	25	Hello Bio	HB0225
NBQX	AMPA receptor antagonist	10	Hello Bio	HB0443
DPDPE	Delta-opioid receptor agonist	0.5	Tocris	J66293-
Naltrindole	Delta-opioid receptor antagonist	0.1	Tocris	0740
ACEA	CB1R agonist	16	Tocris	1319
AM251	CB1R inverse agonist	4	Hello Bio	HB2776
Oxytocin acetate salt	Oxytocin receptor agonist	1 or 10	Bachem	H2510.0025
L-371,257	Oxytocin receptor antagonist	1	Tocris	2410

Histology

After successful whole-cell recordings, slices were fixed in 4% paraformaldehyde (PFA) in phosphate buffered saline (PBS) at 4°C. Post-hoc labeling of filled cells with streptavidin-conjugated Alexa 488 was performed. Slices were permeabilized with 0.2 % Triton in PBS and blocked overnight with 3 % goat serum in PBS with 0.2 % triton. Slices were incubated overnight at 4°C in in 3 % goat serum in PBS, containing streptavidin-conjugated Alexa 488 (Life technologies, used at a 1:300 dilution) and Neurotrace Nissl (Life technologies, used at a 1:300 dilution). Slices were then washed in PBS and mounted. Slices were mounted with Pro-Long Diamond (Thermofisher) and z series confocal images were collected with a Zeiss 710 LSM microscope. Image analysis was performed with ImageJ and cellular morphologies were reconstructed from confocal images.

Biochemical measurements

Mice were divided into two groups: homecage or social interaction. Mice in the homecage group were left undisturbed until sacrificed. Mice in the social interaction group interacted with a novel mouse for 10 minutes and sacrificed 60 minutes after interaction. Finally, brains were extracted and fast-froze in liquid isopentane at -70°C. Samples were kept at -70°C until analyzed. Frozen brains were first mounted on the cryostat stage (Thermo Shandon, France) set at -15°C, then brains were sliced into 200µm-thick slices and bilateral CA1, CA2 and DG punches were collected on each slice and kept on carbon ice until storage at -70°C. RNA from brain punches was extracted using Trizol Reagent™ (Thermofisher Scientific), then extracted RNA underwent several cleaning cycles with ethanol before storage at -20°C. Purity and concentration of total RNA were assessed by absorbance readings (Ratio A260/A230 and A260/A280) using the NanoDrop ND-1000 spectrophotometer (Thermo Fisher Scientific, Wilmington, DE). Then, RNA was reverse transcribed into cDNA using random primers and Transcriptase inverse SuperScript IVTM (Fisher scientific).

Gene amplification was performed using an SYBR Green I Master kit (ref RR420L, TAKARA BIO Europe, France) and appropriate custom primers. Primers for OTR, Wfs1, Rgs14, Actin, Gapdh and Rpl19 were designed and purchased from Eurofins Genomics (France; see below). Amplification reactions were run in duplicate using the LightCycler 480 system (Roche Diagnostics). First, primers accuracy was validated with a standard curve of four serial dilution points of whole hippocampus cDNA pool (ranging from 1000 pg to 1 pg of

total RNA reverse transcripts), and a no template control (NTC). Tm calling curves were examined to verify the specificity of the amplified genes. To estimate CA1 and CA2 enrichment after punches, specific markers of the areas were quantified, using respectively Wfs1 (Luuk et al., 2008) and Rgs14 (Kohara et al., 2014). Three internal control genes, Actin, Gapdh and Rpl19 were quantified for accurate normalization of data. Normalization to reference genes and relative quantities determination were done using GenEx™MultiD software.

OTR: AAAGGAAGGCTAGGGCTAACAGA(F), AGTGCCTATTTGCAGCCTTCA(Rev)

Wfs1: TCAGCAGTGAATCCAAGAACTACAT(F), GAATGATGCCCTTGGCGTACT(Rev)

Rgs14: CCTTTGTGAGCAGCAAATCTGA(F), CTCTCGCTCTCACTCTCTCCACTT(Rev)

Actin: AGTACGATGAGTCCGGCCCCT(F), AACGCAGCTCAGTAACAGTCCGC(Rev)

Gapdh: GAACATCATCCCTGCATCCA(F), CCAGTGAGCTTCCCGTTCA(Rev)

Rpl19: CCCGTCAGCAGATCAGGAA(F), GTCACAGGCTTGCGGATGA(Rev)

Reconstruction and analysis of PNs

PNs were reconstructed using Neurolucida software 360 (MBF Bioscience 2022) using the user-guided “directional kernels” algorithm. Neurolucida Explorer (MBF Bioscience 2022) was used in order to extract quantitative measures. Cell soma location was measured in order to make sure one group did not have a bias in the radial axis.

Sholl analysis (an analysis counting the number of dendritic intersections with a progressively larger concentric circle around the cell soma) was also accomplished through Neurolucida Explorer. 10µm steps were used for the sholl analysis of both basal and apical dendrites. Individual neuron sholl analyses were exported to Python in order to regularize by cell total length percentage (as cell length was highly dependent upon slice mounting) and average plots. This was done by taking the largest cell soma-dendritic end length as reference and doing a linear interpolation of missing data points for the smaller cells.

DREADD viral injections into hippocampal area CA2 and CNO injection

After 7–8 weeks under CD or HFD, CA2-Cre mice were anesthetized with air/isoflurane (4.5% induction; 1.5% maintenance) at 1L/min, injected with the analgesic buprenorphine (Buprécare, 0.1 mg/kg s.c. in 0.9% saline) and the non-steroidal anti-inflammatory drug carproxifen (Carprofène, 20mg/kg s.c. in 0.9% saline) and were placed on a stereotaxic apparatus (David Kopf Instruments). The scalp was shaved, disinfected with 10% povidone iodine and locally anaesthetized with a subcutaneous injection of lidocaine

(Lurocaine 20mg/mL, 0.1ml non diluted). An anterograde adeno-associated virus carrying Cre-dependent inhibitory DREADD (AAV8-hSyn1-dlox-hM4DGi-mCherr) or control virus (AAV8-hSyn1-dlox-mCherry) was infused bilaterally using a 10 µL Hamilton syringe (Hamilton) and an ultra-micro pump (µMP3, World Precision Instruments, USA) over 2 min (100 nL/min) in the dorsal CA2 in each hemisphere (AP -1.5 mm, ML ± 2.4 mm, DV -1.8mm relative to Bregma). The pipette was left in place for a 5 minutes diffusion period, before being slowly removed. The incision was closed with sutures and the animal was kept on a heating pad until recovery. Mice were single housed for 2 days and their body weight and behavior were closely monitored during the 4 days following the procedure. Then, they were housed in groups of 4 to 8 mice per cage and behavioral tests started 4 weeks later, enabling optimal virus expression.

To decrease the activity of CA2 PNs during social memory encoding, mice received an i.p. injection of the exogenous DREADD ligand Clozapine-N-oxyde (CNO, 2 mg/kg dissolved in 0.9% saline) 45 min before the sociability session. After behavior, mCherry expression in CA2 was verified histologically.

Intra-CA2 cannulas implantation and injection procedure

Stainless steel guide cannulae (28-gauge, Plastics One) were implanted bilaterally 1mm above the CA2 (AP -1.5 mm; ML ±2.4 mm; DV -0.8 mm from Bregma). Guide cannulae were maintained in position with dental cement and dummy cannulae were kept in each guide at all times except during micro-infusions. Mice were allowed at least 5 days to recover from surgery, during which they were handled and weighed daily. The OT (Sigma–Aldrich) was dissolved in saline (0.9% NaCl) to obtain a final concentration of 1ng or 10ng /0.2 µl, corresponding to a concentration of 5µM and 50µM. The vehicle solution was saline. OT or saline was infused by inserting a 33-gauge internal cannula into the guide cannula. The internal cannula was connected to a 1µl glass syringe attached to an infusion pump (Harvard Apparatus) and projected an additional 1 mm ventral to the tip of the guide cannula. A total volume of 0.2µl was delivered bilaterally at a rate of 0.1 µl/min. The internal cannula remained in place for a further 1 min after the infusions and was then removed. The concentration, rate and infusion volumes were chosen based on previous literature (Ferguson et al., 2001; Lukas et al., 2011; Lahoud and Maroun, 2013).

All mice were sacrificed after behavioral testing. Animals were deeply anaesthetized with a mix of pentobarbital and lidocaine (Exagon, 300 mg/ kg and Lurocaine, 30 mg/kg)

before cardiac perfusion with phosphate-buffered saline solution followed by 4% paraformaldehyde (Sigma-Aldrich) diluted in phosphate-buffered saline. Brains were collected and post-fixed in 4% paraformaldehyde at 4°C, then stored at 4°C until slicing. 40μm coronal sections were cut on a vibratome (Leica) and stored in cryoprotective solution (glycerol and ethylene glycol; Sigma-Aldrich) at −20°C. Every sixth section was mounted on gelatin-coated slides, covered by medium (Southern Biotech) and cover-slipped. The slices were visualized under a microscope and each section was photographed (Nikon-ACT-1 software), enabling assessment of correct cannula implantation.

Test for sociability and SRM

CD and HFD-fed mice behavior was assessed in an open-field Plexiglas arena (45 × 25 cm and 20 cm high) placed in a sound attenuated room adapted from (Okuyama et al., 2016; Rani et al., 2021). The assay paradigm comprises three sessions: habituation, training, and test. In the first session, mice were placed in the arena containing two empty pencil-wire cups positioned on opposing sides and left free to explore for 10 min. Then, 24 h after this session, a juvenile mouse (stimulus, 6−7 weeks old), which had no prior contact with the subject mice, was placed under one of the wire cups while the other cup remained empty. The subject mouse was then placed in the arena and was left free to explore it for 10 min. During the third session, performed either 15 minutes or 3 hours later, the same stimulus animal was again placed under the wire cup and a novel unfamiliar juvenile mouse was placed under the opposing cup. Experimental mice were then placed again in the arena and tested for discrimination between novel and familiar mouse in a 10 min session. Each experimental mouse was subjected to the procedure separately, and care was taken to remove any olfactory/taste cues by cleaning carefully the arena and wire cups between trials. The positions of the social stimuli (empty × social; familiar × novel) were counterbalanced across subjects and trials to prevent bias due to place preference. All juvenile stimulus mice were habituated to remain under the wire cups for 30 min during several days before behavioral testing. The animal's behavior during all sessions was videotaped, and the time spent actively exploring the stimuli was analyzed by experienced observers unaware of the experimental groups. Exploration was defined as direct snout-to-cup contact, and the time spent climbing on the cups was not considered. Data are expressed as a percentage of time spent exploring each cup (social × non-social during the second session or familiar × novel during the third session). The raw exploration time data were also employed to determine social and discrimination indexes, according to the following equations: Sociability index = (time

exploring social cup- time exploring non-social cup)/ total exploration time of both cups; Discrimination Index = (time exploring novel mouse- time exploring familiar mouse)/ total time of exploration of both mice).

Test for social discrimination between cagemate and novel mouse

The assay paradigm was similar to the one above used for SRM but comprises only two sessions: habituation and discrimination test. In the first session, mice were placed the arena containing two empty pencil-wire cups positioned on opposite sides and left free to explore for 10 min. Then, 24 h after this session, the subject mouse was placed in the arena again and left free to explore for 10 min two mice placed under the wire cups. One mouse (novel) never had contact with the subject and the other mouse was a familiar co-housed littermate of the subject mouse (cagemate). Novel and cagemate stimulus mice were habituated to remain under the wire cups for 30 min the day before behavioral testing. Data are expressed as Discrimination Index = (time exploring novel mouse- time exploring cagemate)/ total time of exploration of both mice).

Object recognition memory

During training, two identical new objects were presented in a novel open field arena (40 × 40 × 40 cm, wood) and each mouse was left freely to explore them. Long-term memory was assessed 24 hours later, by randomly replacing one of the objects by a novel one. In both phases, object exploration, defined as nose and whiskers pointed towards the object in a distance of less than 1–1.5 cm away, was quantified by a trained experimenter blind to experimental groups. In both phases, the session duration was 10 min max but the mouse was removed from the apparatus after 20 s of total exploration for both objects which reduces inter-individual variability (Leger et al., 2013), otherwise mice were excluded from analysis. Data are presented as the percentage of exploration of novel object over total exploration time of both objects.

Data analysis and statistics

Origin Pro software was used for electrophysiology data analysis and statistics. The Shapiro-Wilk test was used to determine whether the data followed a normal distribution and an F-test to see if was homoscedastic. We used Student's t tests (two-sample or paired-sample) and 2-way ANOVAs when the data followed a normal distribution and were of equal variance. When the distribution was not normal or the variances unequal, we used non-

parametric tests (Mann-Whitney, Friedman test). Statistical significance was set to $p < 0.05$ (*** indicates $p < 0.001$, ** indicates $p < 0.01$, and * indicates $p < 0.05$). All values are reported as the mean ± SEM.

Bibliography

Abbott KN, Arnott CK, Westbrook RF, Tran DMD. 2019. The effect of high fat, high sugar, and combined high fat-high sugar diets on spatial learning and memory in rodents: A meta-analysis. Neuroscience and Biobehavioral Reviews [Internet] 107:399–421. Available from: https://doi.org/10.1016/j.neubiorev.2019.08.010

Alfaris N, Alqahtani AM, Alamuddin N, Rigas G. 2023. Global Impact of Obesity. Gastroenterology Clinics of North America [Internet] 52:277–293. Available from: https://www.sciencedirect.com/science/article/pii/S0889855323000286

Blüher M. 2019. Obesity: global epidemiology and pathogenesis. Nature Reviews Endocrinology 15:288–298.

Chen S, He L, Huang AJY, Boehringer R, Robert V, Wintzer ME, Polygalov D, Weitemier AZ, Tao Y, Gu M, Middleton SJ, Namiki K, Hama H, Therreau L, Chevaleyre V, Hioki H, Miyawaki A, Piskorowski RA, McHugh TJ. 2020. A hypothalamic novelty signal modulates hippocampal memory. Nature 586:270–274.

Chevaleyre V, Siegelbaum SA. 2010. Strong CA2 pyramidal neuron synapses define a powerful disynaptic cortico-hippocampal loop. Neuron 66:560–572.

Chooi YC, Ding C, Magkos F. 2019. The epidemiology of obesity. Metabolism [Internet] 92:6–10. Available from: https://www.sciencedirect.com/science/article/pii/S002604951830194X

Cordner ZA, Tamashiro KLK. 2015. Effects of high-fat diet exposure on learning & memory. Physiology and Behavior [Internet] 152:363–371. Available from: http://dx.doi.org/10.1016/j.physbeh.2015.06.008

Di Marzo V. 2008. The endocannabinoid system in obesity and type 2 diabetes. Diabetologia [Internet] 51:1356–1367. Available from: https://link.springer.com/article/10.1007/s00125-008-1048-2

Dutta S, Sengupta P. 2016. Men and mice: Relating their ages. Life sciences 152:244–248.

Fadó R, Molins A, Rojas R, Casals N. 2022. Feeding the Brain: Effect of Nutrients on Cognition, Synaptic Function, and AMPA Receptors. Nutrients 14:1–36.

Farsetti E, Amato S, Averna M, Guidolin D, Pedrazzi M, Maura G, Agnati LF, Cervetto C, Marcoli M. 2025. Dual Oxytocin Signals in Striatal Astrocytes. Biomolecules [Internet] 15:1122. Available from: https://www.mdpi.com/2218-273X/15/8/1122

Ferguson JN, Aldag JM, Insel TR, Young LJ. 2001. Oxytocin in the Medial Amygdala is Essential for Social Recognition in the Mouse. J Neurosci [Internet] 21:8278. Available from: http://www.jneurosci.org/content/21/20/8278.abstract

Hayashi R, Kasahara Y, Hidema S, Fukumitsu S, Nakagawa K, Nishimori K. 2020. Oxytocin Ameliorates Impaired Behaviors of High Fat Diet-Induced Obese Mice. Frontiers in Endocrinology [Internet] 11:379–379. Available from: www.frontiersin.org

Hitti FL, Siegelbaum SA. 2014. The hippocampal CA2 region is essential for social memory. Nature 508:88–92.

Kerem L, Lawson EA. 2021. The effects of oxytocin on appetite regulation, food intake and metabolism in humans. International Journal of Molecular Sciences 22.

Khazen T, Hatoum OA, Ferreira G, Maroun M. 2019. Acute exposure to a high-fat diet in juvenile male rats disrupts hippocampal-dependent memory and plasticity through glucocorticoids. Scientific Reports 9:1–10.

Khazen T, Narattil NR, Ferreira G, Maroun M. 2022. Hippocampal oxytocin is involved in spatial memory and synaptic plasticity deficits following acute high-fat diet intake in juvenile rats. Cerebral cortex (New York, NY□: 1991) [Internet]. Available from: https://pubmed.ncbi.nlm.nih.gov/35989314/

Kohara K, Pignatelli M, Rivest AJ, Jung H-Y, Kitamura T, Suh J, Frank D, Kajikawa K, Mise N, Obata Y, Wickersham IR, Tonegawa S. 2014. Cell type–specific genetic and optogenetic tools reveal hippocampal CA2 circuits. Nat Neurosci 17:269–279.

Lahoud N, Maroun M. 2013. Oxytocinergic manipulations in corticolimbic circuit differentially affect fear acquisition and extinction. Psychoneuroendocrinology [Internet] 38:2184–2195. Available from: https://www.sciencedirect.com/science/article/pii/S0306453013001248

Leger M, Quiedeville A, Bouet V, Haelewyn B, Boulouard M, Schumann-Bard P, Freret T. 2013. Object recognition test in mice. Nat Protoc [Internet] 8:2531–2537. Available from: https://www.nature.com/articles/nprot.2013.155

Lin Y-T, Hsieh T-Y, Tsai T-C, Chen C-C, Huang C-C, Hsu K-S. 2018. Conditional Deletion of Hippocampal CA2/CA3a Oxytocin Receptors Impairs the Persistence of Long-Term Social Recognition Memory in Mice. The Journal of neuroscience□: the official journal of the Society for Neuroscience 38:1218–1231.

Liu J-J, Eyring KW, König GM, Kostenis E, Tsien RW. 2022. Oxytocin-Modulated Ion Channel Ensemble Controls Depolarization, Integration and Burst Firing in CA2 Pyramidal Neurons. The Journal of neuroscience□: the official journal of the Society for Neuroscience 42:7707–7720.

Loisy M, Bouisset G, Lopez S, Muller M, Spitsyn A, Duval J, Piskorowski RA, Verret L, Chevaleyre V. 2022. Sequential inhibitory plasticities in hippocampal area CA2 and social memory formation. Neuron 110:2854-2866.e4.

Loisy M, Farah A, Fafouri A, Fanton A, Ahmadi M, Therreau L, Chevaleyre V, Piskorowski RA. 2023. Environmental enrichment and social isolation modulate inhibitory transmission and plasticity in hippocampal area CA2. Hippocampus [Internet] 33:197–207. Available from: https://onlinelibrary.wiley.com/doi/abs/10.1002/hipo.23478

Lopez-Rojas J, De Solis CA, Leroy F, Kandel ER, Siegelbaum SA. 2022. A direct lateral entorhinal cortex to hippocampal CA2 circuit conveys social information required for social memory. Neuron [Internet] 110:1559-1572.e4. Available from: https://linkinghub.elsevier.com/retrieve/pii/S089662732200085X

Loprinzi PD, Frith E. 2018. Obesity and episodic memory function. Journal of Physiological Sciences [Internet] 68:321–331. Available from: https://doi.org/10.1007/s12576-018-0612-x

Lukas M, Toth I, Reber SO, Slattery DA, Veenema AH, Neumann ID. 2011. The Neuropeptide Oxytocin Facilitates Pro-Social Behavior and Prevents Social Avoidance in Rats and Mice. Neuropsychopharmacol [Internet] 36:2159–2168. Available from: https://www.nature.com/articles/npp201195

Luuk H, Koks S, Plaas M, Hannibal J, Rehfeld JF, Vasar E. 2008. Distribution of Wfs1 protein in the central nervous system of the mouse and its relation to clinical symptoms of the Wolfram syndrome. J of Comparative Neurology 509:642–660.

Martin AA, Davidson TL. 2014. Human cognitive function and the obesogenic environment. Physiology and Behavior [Internet] 136:185–193. Available from: /pmc/articles/PMC4161661/?report=abstract

Massa F, Mancini G, Schmidt H, Steindel F, Mackie K, Angioni C, Oliet SHR, Geisslinger G, Lutz B. 2010. Alterations in the hippocampal endocannabinoid system in diet-induced obese mice. Journal of Neuroscience 30:6273–6281.

Meinung C-P, Boi L, Pandamooz S, Mazaud D, Ghézali G, Rouach N, Neumann ID. 2025. OXTR-mediated signaling in astrocytes contributes to anxiolysis. Mol Psychiatry [Internet] 30:2620–2634. Available from: https://www.nature.com/articles/s41380-024-02870-5

Meira T, Leroy F, Buss EW, Oliva A, Park J, Siegelbaum SA. 2018. A hippocampal circuit linking dorsal CA2 to ventral CA1 critical for social memory dynamics. Nature communications 9:1–14.

Okuyama T, Kitamura T, Roy DS, Itohara S, Tonegawa S. 2016. Ventral CA1 neurons store social memory. Science [Internet] 353:1536–1541. Available from: https://www.science.org/doi/10.1126/science.aaf7003

Oliva A, Fernández-Ruiz A, Leroy F, Siegelbaum SA. 2020. Hippocampal CA2 sharp-wave ripples reactivate and promote social memory. Nature:1–6.

Pagani JH, Zhao M, Cui Z, Avram SKW, Caruana DA, Dudek SM, Young WS. 2014. Role of the vasopressin 1b receptor in rodent aggressive behavior and synaptic plasticity in hippocampal area CA2. Molecular psychiatry 20:490–499.

Pan L, Zheng L, Wu X, Zhu Z, Wang S, Lu Y, He Y, Yang Q, Ma X, Wang X, Yang H, Zhan L, Luo Y, Li X, Zhou Y, Wang X. 2022. A short period of early life oxytocin treatment rescues social behavior dysfunction via suppression of hippocampal hyperactivity in male mice. Molecular Psychiatry:1–15.

Pimpinella D, Mastrorilli V, Giorgi C, Coemans S, Lecca S, Lalive AL, Ostermann H, Fuchs EC, Monyer H, Mele A, Cherubini E, Griguoli M. 2021. Septal cholinergic input to CA2 hippocampal region controls social novelty discrimination via nicotinic receptor-mediated disinhibition. eLife 10:e65580.

Popik P, Vetulani J. 1991. Opposite action of oxytocin and its peptide antagonists on social memory in rats. Neuropeptides [Internet] 18:23–27. Available from: https://www.sciencedirect.com/science/article/pii/014341799190159G

Popik P, Vetulani J, Van Ree JM. 1992. Low doses of oxytocin facilitate social recognition in rats. Psychopharmacology [Internet] 106:71–74. Available from: http://link.springer.com/10.1007/BF02253591

Raam T, McAvoy KM, Besnard A, Veenema A, Sahay A. 2017. Hippocampal oxytocin receptors are necessary for discrimination of social stimuli. Nature communications 8:2001.

Rani B, Silva-Marques B, Leurs R, Passani MB, Blandina P, Provensi G. 2021. Short- and Long-Term Social Recognition Memory Are Differentially Modulated by Neuronal Histamine. Biomolecules [Internet] 11. Available from: https://www.mdpi.com/2218-273X/11/4/555

Reichelt AC, Gibson GD, Abbott KN, Hare DJ. 2019. A high-fat high-sugar diet in adolescent rats impairs social memory and alters chemical markers characteristic of atypical neuroplasticity and parvalbumin interneuron depletion in the medial prefrontal cortex. Food and Function 10:1985–1998.

Rivera P, Luque-Rojas MJ, Pastor A, Blanco E, Pavón FJ, Serrano A, Crespillo A, Vida M, Grondona JM, Cifuentes M, Bermúdez-Silva FJ, de la Torre R, de Fonseca FR, Suárez J. 2013. Diet-dependent modulation of hippocampal expression of endocannabinoid signaling-related proteins in cannabinoid antagonist-treated obese rats. European Journal of Neuroscience [Internet] 37:105–117. Available from: http://doi.wiley.com/10.1111/ejn.12012

Sarfert KS, Knabe ML, Gunawansa NS, Blythe SN. 2019. Western-style diet induces object recognition deficits and alters complexity of dendritic arborization in the hippocampus and entorhinal cortex of male rats. Nutritional Neuroscience 22:344–353.

Stevenson EL, Caldwell HK. 2014. Lesions to the CA2 region of the hippocampus impair social memory in mice. European Journal of Neuroscience 40.

Takase K, Tsuneoka Y, Oda S, Kuroda M, Funato H. 2016. High-fat diet feeding alters olfactory-, social-, and reward-related behaviors of mice independent of obesity. Obesity [Internet] 24:886–894. Available from: https://onlinelibrary-wiley-com.proxy.insermbiblio.inist.fr/doi/full/10.1002/oby.21441

Thirtamara Rajamani K, Barbier M, Lefevre A, Niblo K, Cordero N, Netser S, Grinevich V, Wagner S, Harony-Nicolas H. 2024. Oxytocin activity in the paraventricular and supramammillary nuclei of the hypothalamus is essential for social recognition memory in rats. Mol Psychiatry [Internet] 29:412–424. Available from: https://www.nature.com/articles/s41380-023-02336-0

Tirko NN, Eyring KW, Carcea I, Mitre M, Chao MV, Froemke RC, Tsien RW. 2018. Oxytocin Transforms Firing Mode of CA2 Hippocampal Neurons. Neuron 100:593-608.e3.

Tsai T-C, Fang Y-S, Hung Y-C, Hung L-C, Hsu K-S. 2022. A dorsal CA2 to ventral CA1 circuit contributes to oxytocinergic modulation of long-term social recognition memory. Journal of Biomedical Science 29:50.

Tsan L, Décarie-Spain L, Noble EE, Kanoski SE. 2021. Western Diet Consumption During Development: Setting the Stage for Neurocognitive Dysfunction. Frontiers in Neuroscience [Internet] 15. Available from: https://www.frontiersin.org/journals/neuroscience/articles/10.3389/fnins.2021.632312

Wahis J, Baudon A, Althammer F, Kerspern D, Goyon S, Hagiwara D, Lefevre A, Barteczko L, Boury-Jamot B, Bellanger B, Abatis M, Gouveia MDS, Benusiglio D, Eliava M, Rozov A, Weinsanto I, Knobloch-Bollmann HS, Kirchner MK, Roy RK, Wang H, Pertin M, Inquimbert P, Pitzer C, Siemens J, Goumon Y, Boutrel B, Lamy CM, Decosterd I, Chatton J-Y, Rouach N, Young WS, Stern JE, Poisbeau P, Stoop R, Darbon P, Grinevich V, Charlet A. 2021. Astrocytes mediate the effect of oxytocin in the central amygdala on neuronal activity and affective states in rodents. Nature Neuroscience 24:529–541.

Wei D, Lee DY, Cox CD, Karsten CA, Penagarikano O, Geschwind DH, Gall CM, Piomelli D. 2015. Endocannabinoid signaling mediates oxytocin-driven social reward. Proceedings of the National Academy of Sciences of the United States of America 112:14084–14089.

Wu H, Zhang W, Huang M, Lin X, Chiou J. 2023. Prolonged High-Fat Diet Consumption throughout Adulthood in Mice Induced Neurobehavioral Deterioration via Gut-Brain Axis. Nutrients 2023, Vol 15, Page 392 [Internet] 15:392–392. Available from: https://www.mdpi.com/2072-6643/15/2/392/htm

Wu L, Meng J, Shen Q, Zhang Y, Pan S, Chen Z, Zhu LQ, Lu Y, Huang Y, Zhang G. 2017. Caffeine inhibits hypothalamic A1R to excite oxytocin neuron and ameliorate dietary obesity in mice. Nature Communications 2017 8:1 [Internet] 8:1–15. Available from: https://www-nature-com.proxy.insermbiblio.inist.fr/articles/ncomms15904

Yaseen A, Shrivastava K, Zuri Z, Hatoum OA, Maroun M. 2019. Prefrontal Oxytocin is Involved in Impairments in Prefrontal Plasticity and Social Memory Following Acute Exposure to High Fat Diet in Juvenile Animals. Cerebral Cortex 29:1900–1909.

Yeomans MR. 2017. Adverse effects of consuming high fat-sugar diets on cognition: implications for understanding obesity. Proceedings of the Nutrition Society 76:455–465.

Zhan S, Qi Z, Cai F, Gao Z, Xie J, Hu J. 2024. Oxytocin neurons mediate stress-induced social memory impairment. Current Biology [Internet] 34:36-45.e4. Available from: https://www.sciencedirect.com/science/article/pii/S0960982223015877

Zhang G, Cai D. 2011. Circadian intervention of obesity development via resting-stage feeding manipulation or oxytocin treatment. American Journal of Physiology - Endocrinology and Metabolism [Internet] 301:E1004–E1004. Available from: /pmc/articles/PMC3214005/

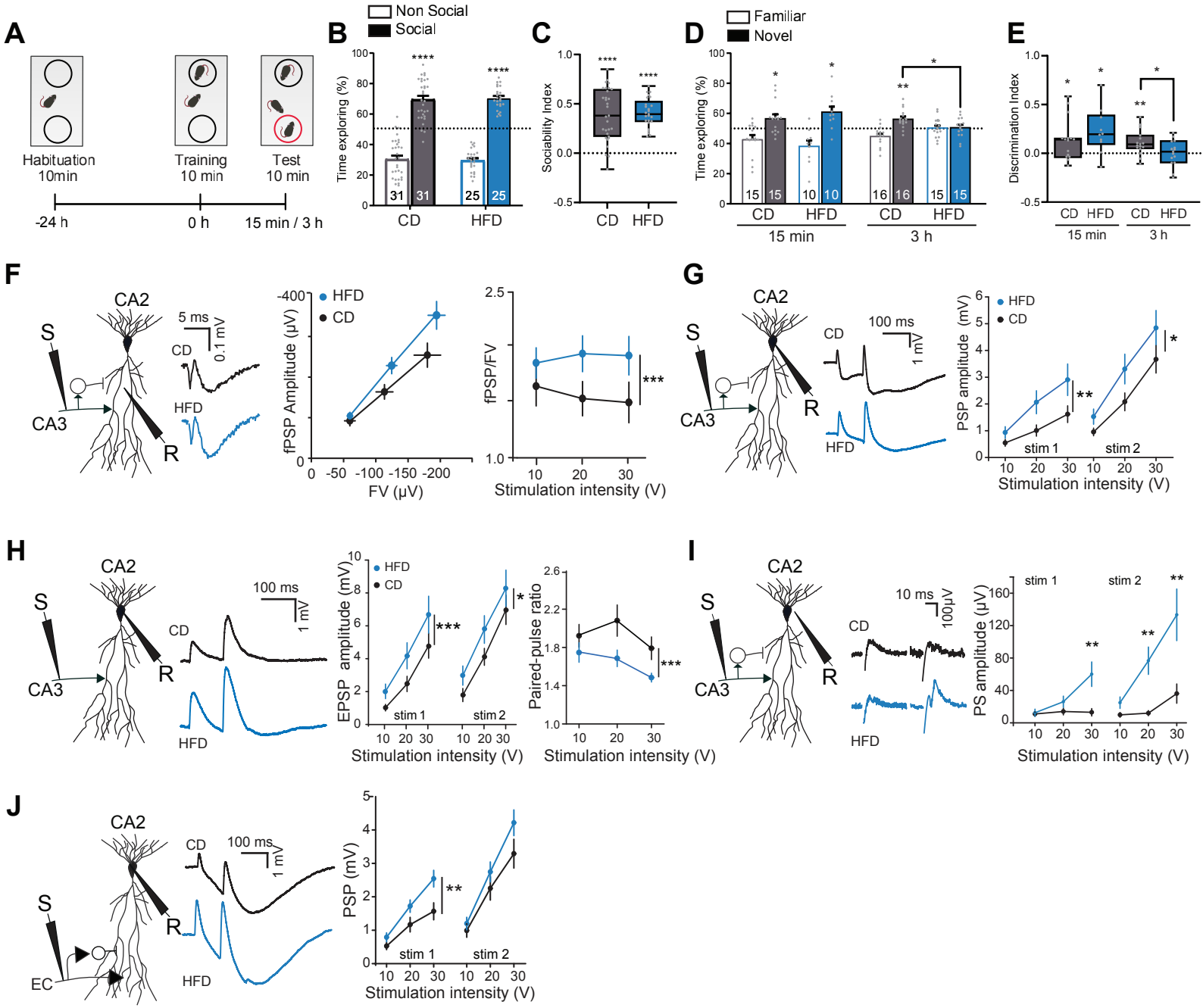
A
Habituation
10min
Training
10 min
Test
10 min
-24 h
0 h
15 min / 3 h
B
Non Social
Social
Time exploring (%)
CD
HFD
C
Sociability Index
CD
HFD
D
Familiar
Novel
Time exploring (%)
CD
HFD
CD
HFD
15 min
3 h
E
Discrimination Index
CD
HFD
CD
HFD
15 min
3 h
F
S
CA2
CA3
R
5 ms
0.1 mV
CD
HFD
fPSP Amplitude (μV)
HFD
CD
FV (μV)
fPSP/FV
Stimulation intensity (V)
G
S
CA2
CA3
R
CD
100 ms
1 mV
HFD
PSP amplitude (mV)
HFD
CD
stim 1
stim 2
Stimulation intensity (V)
H
S
CA2
CA3
R
CD
100 ms
1 mV
HFD
EPSP amplitude (mV)
HFD
CD
stim 1
stim 2
Stimulation intensity (V)
Paired-pulse ratio
Stimulation intensity (V)
I
S
CA2
CA3
R
CD
10 ms
100μV
HFD
PS amplitude (μV)
stim 1
stim 2
Stimulation intensity (V)
J
S
CA2
EC
R
CD
100 ms
1 mV
HFD
PSP (mV)
stim 1
stim 2
Stimulation intensity (V)

Figure 1.

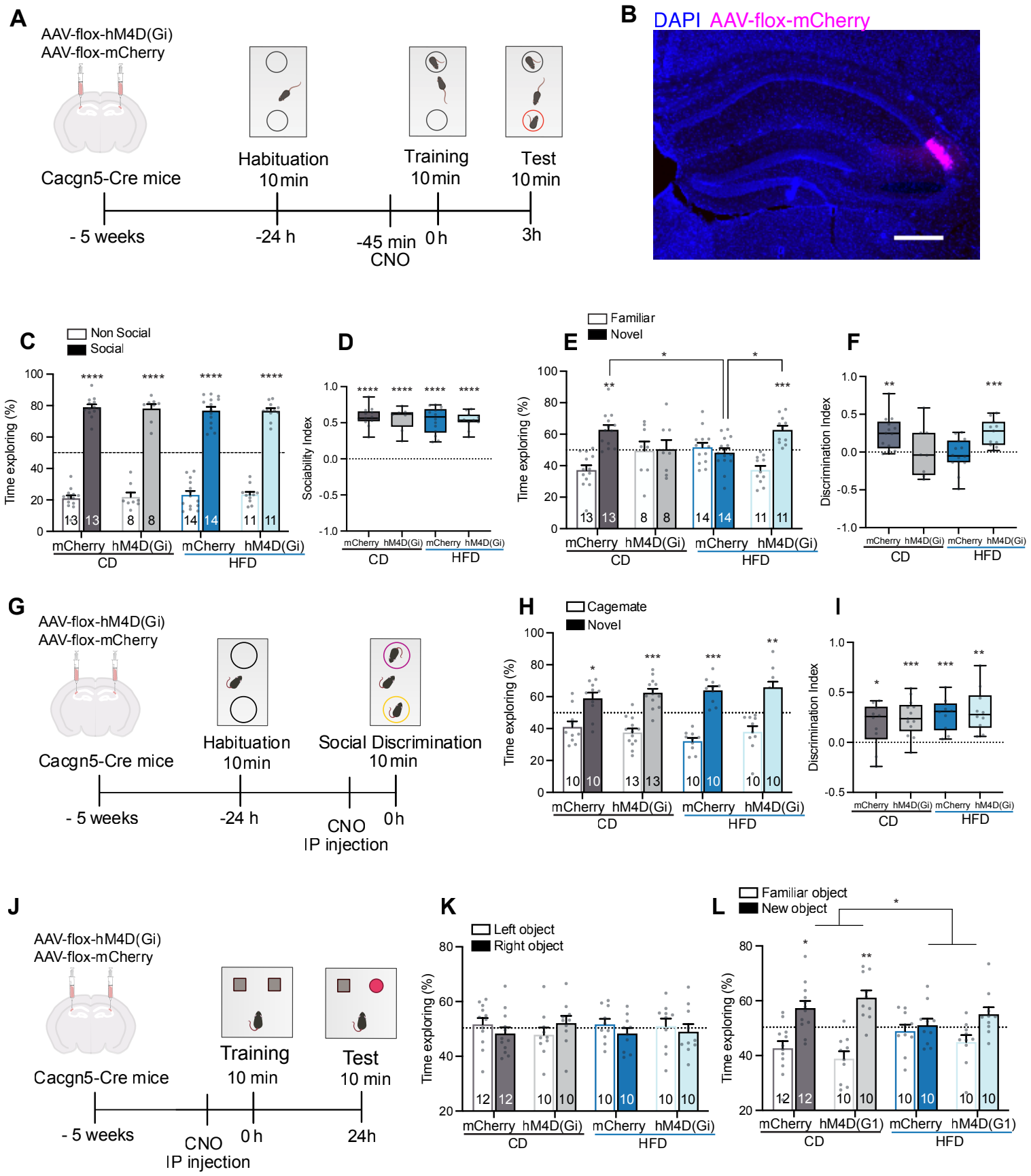
A
AAV-flox-hM4D(Gi)
AAV-flox-mCherry
Cacgn5-Cre mice
Habituation
10 min
Training
10 min
Test
10 min
- 5 weeks
-24 h
-45 min
CNO
0 h
3h
B
DAPI AAV-flox-mCherry
C
Non Social
Social
Time exploring (%)
mCherry hM4D(Gi) mCherry hM4D(Gi)
CD
HFD
D
Sociability Index
E
Familiar
Novel
F
Discrimination Index
G
Habituation
10min
Social Discrimination
10 min
CNO
IP injection
H
Cagemate
Novel
I
J
Training
10 min
Test
10 min
K
Left object
Right object
L
Familiar object
New object
mCherry hM4D(G1)

Figure 2

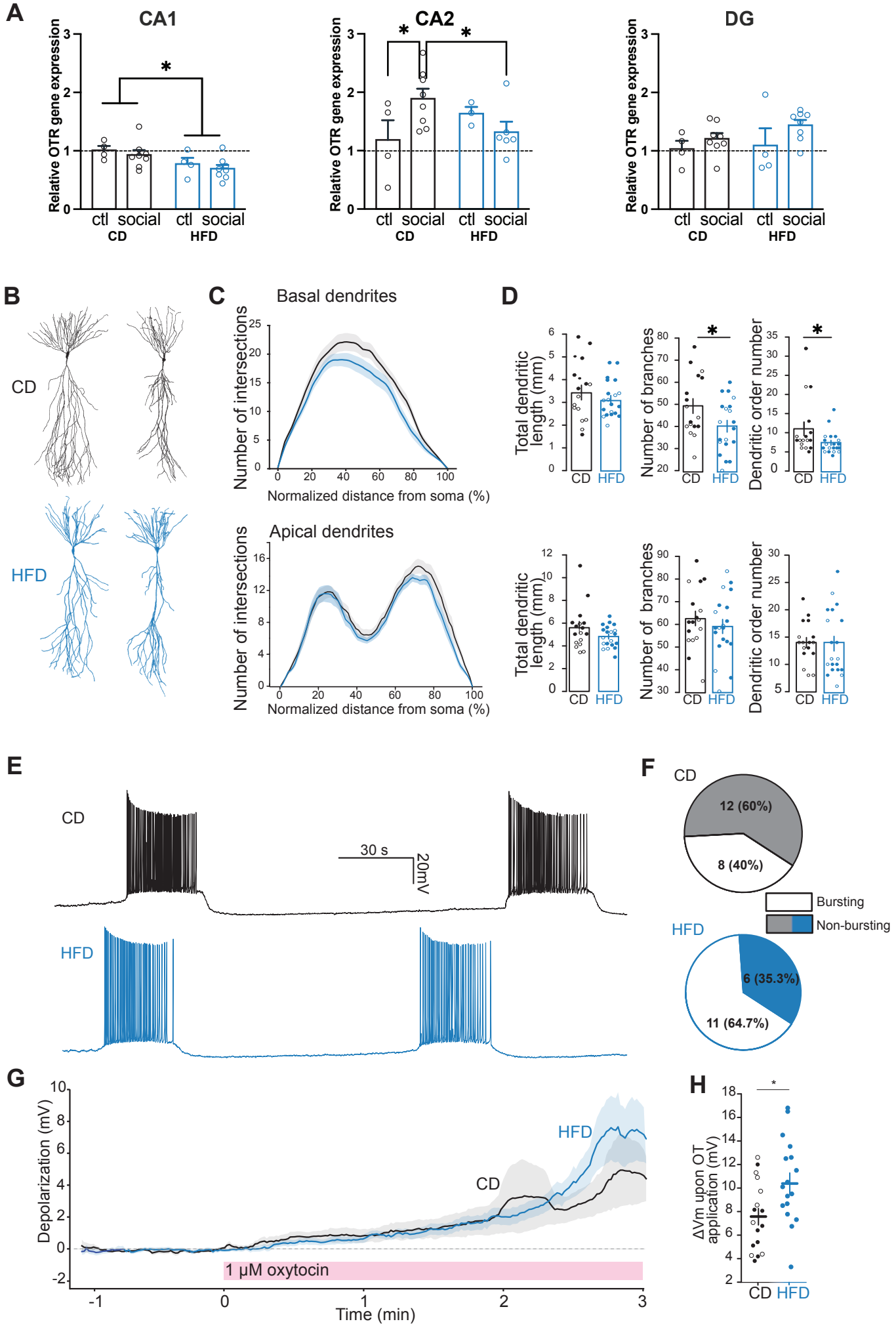
A
CA1
CA2
DG
Relative OTR gene expression
ctl
social
CD
HFD
B
CD
HFD
C
Basal dendrites
Apical dendrites
Number of intersections
Normalized distance from soma (%)
D
Total dendritic length (mm)
Number of branches
Dendritic order number
E
CD
HFD
30 s
20mV
F
CD
12 (60%)
8 (40%)
Bursting
Non-bursting
HFD
6 (35.3%)
11 (64.7%)
G
Depolarization (mV)
HFD
CD
1 μM oxytocin
Time (min)
H
ΔVm upon OT application (mV)

Figure 3

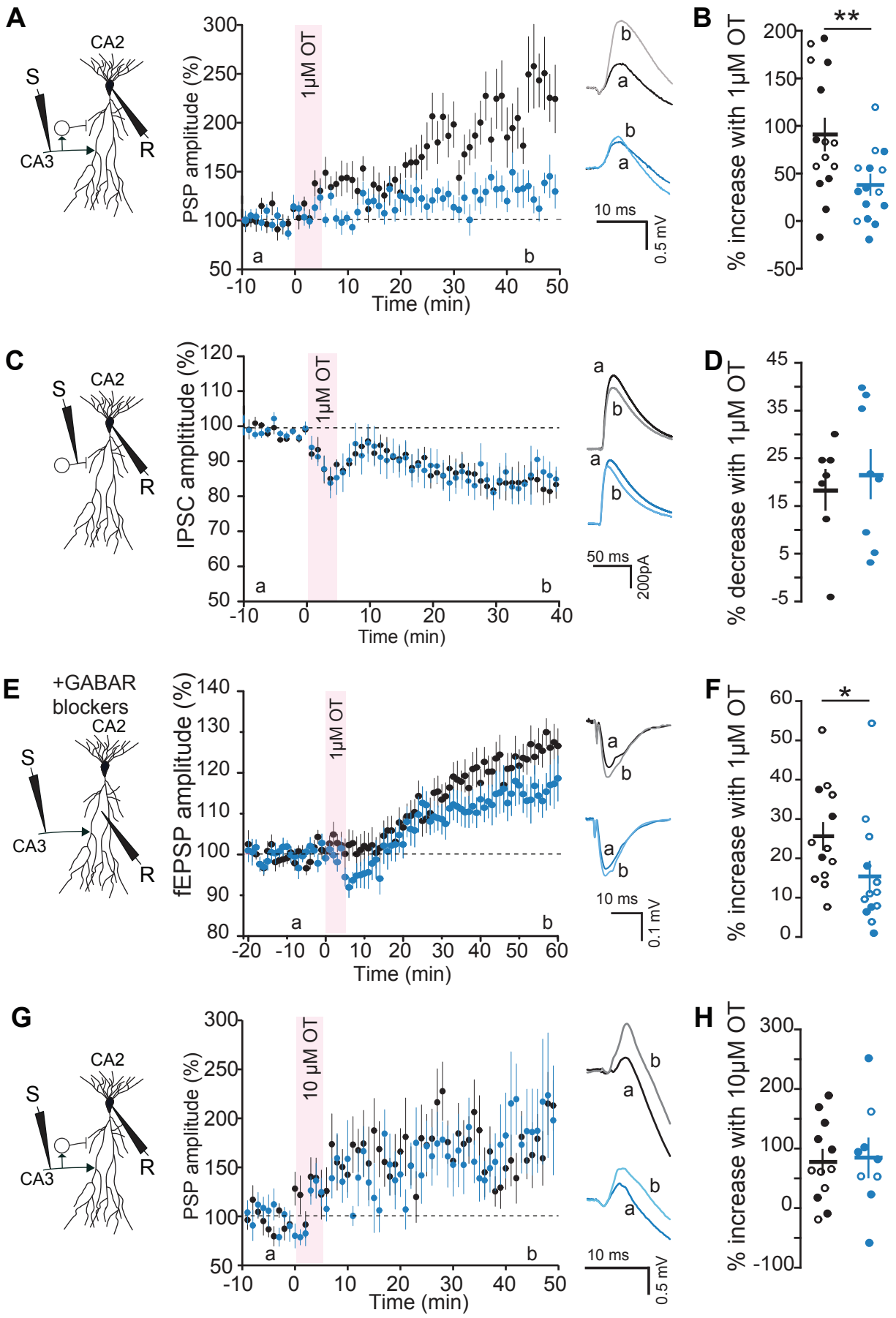
A
CA2
S
CA3
R
PSP amplitude (%)
1μM OT
Time (min)
a
b
10 ms
0.5 mV
B
% increase with 1μM OT
**
C
IPSC amplitude (%)
50 ms
200pA
D
% decrease with 1μM OT
E
+GABAR blockers
fEPSP amplitude (%)
0.1 mV
F
*
G
10 μM OT
H
% increase with 10μM OT

Figure 4.

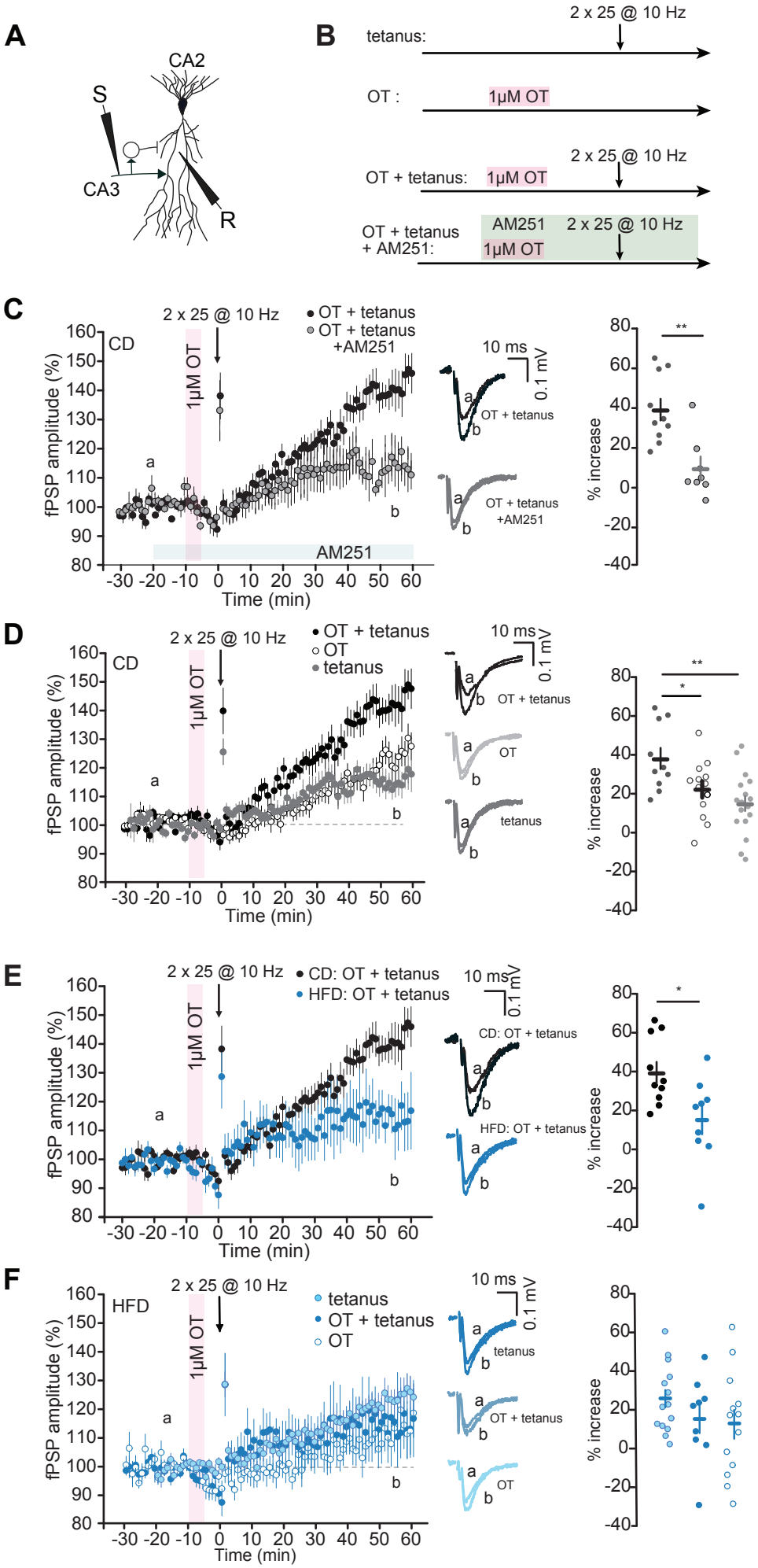
A
CA2
S
CA3
R
B
tetanus:
2 x 25 @ 10 Hz
OT :
1μM OT
OT + tetanus:
1μM OT
2 x 25 @ 10 Hz
OT + tetanus
+ AM251:
AM251
1μM OT
2 x 25 @ 10 Hz
C
CD
2 x 25 @ 10 Hz
1μM OT
OT + tetanus
OT + tetanus
+AM251
AM251
fPSP amplitude (%)
Time (min)
10 ms
0.1 mV
OT + tetanus
OT + tetanus
+AM251
% increase
D
CD
2 x 25 @ 10 Hz
1μM OT
OT + tetanus
OT
tetanus
fPSP amplitude (%)
Time (min)
10 ms
0.1 mV
OT + tetanus
OT
tetanus
% increase
E
2 x 25 @ 10 Hz
1μM OT
CD: OT + tetanus
HFD: OT + tetanus
fPSP amplitude (%)
Time (min)
10 ms
0.1 mV
CD: OT + tetanus
HFD: OT + tetanus
% increase
F
HFD
2 x 25 @ 10 Hz
1μM OT
tetanus
OT + tetanus
OT
fPSP amplitude (%)
Time (min)
10 ms
0.1 mV
tetanus
OT + tetanus
OT
% increase

Figure 5

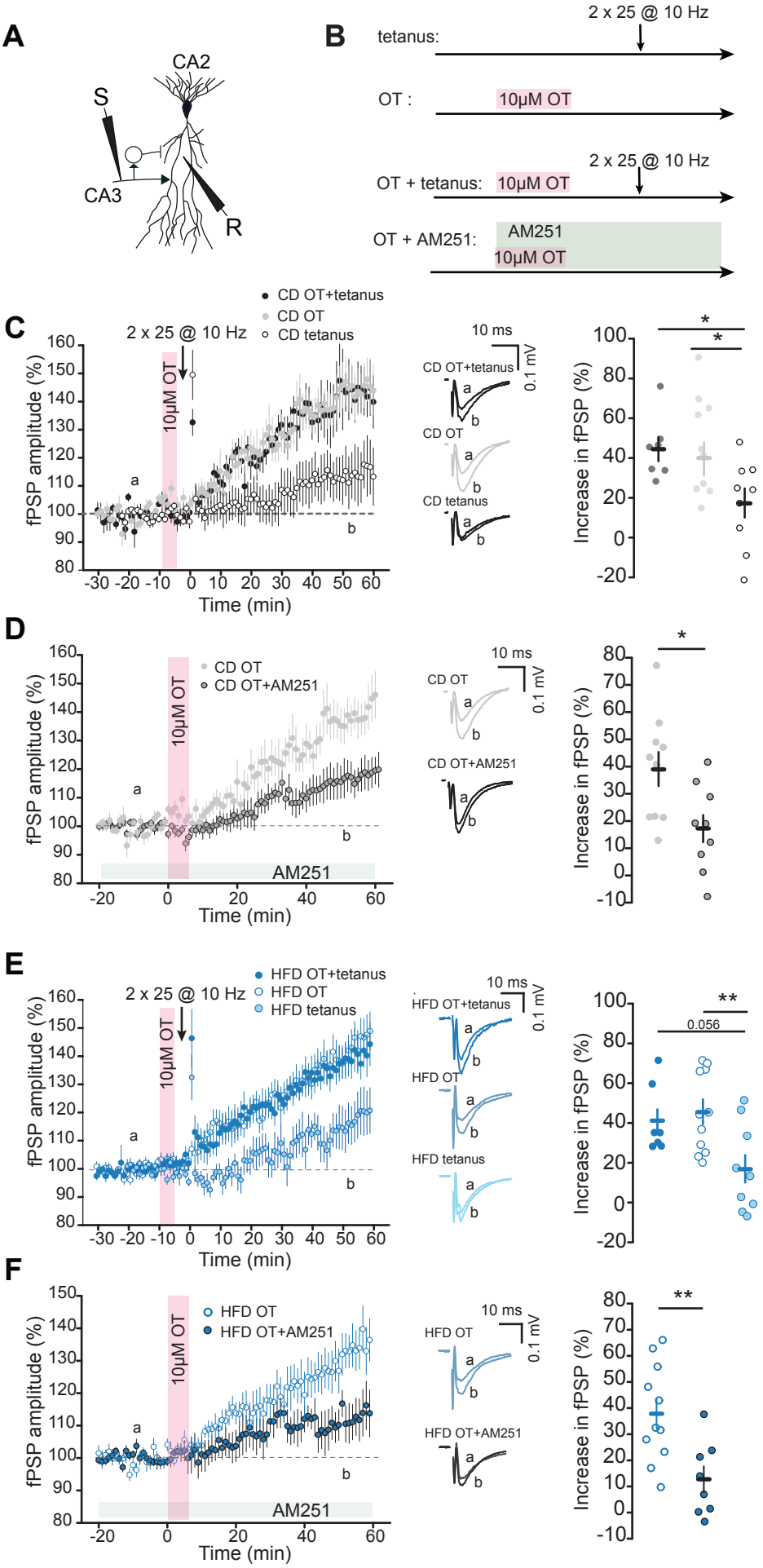
A
CA2
S
CA3
R
B
tetanus:
2 x 25 @ 10 Hz
OT :
10μM OT
OT + tetanus:
10μM OT
2 x 25 @ 10 Hz
OT + AM251:
AM251
10μM OT
C
CD OT+tetanus
CD OT
CD tetanus
2 x 25 @ 10 Hz
10μM OT
fPSP amplitude (%)
Time (min)
10 ms
0.1 mV
Increase in fPSP (%)
D
CD OT
CD OT+AM251
AM251
E
HFD OT+tetanus
HFD OT
HFD tetanus
0.056
F
HFD OT
HFD OT+AM251

Figure 6

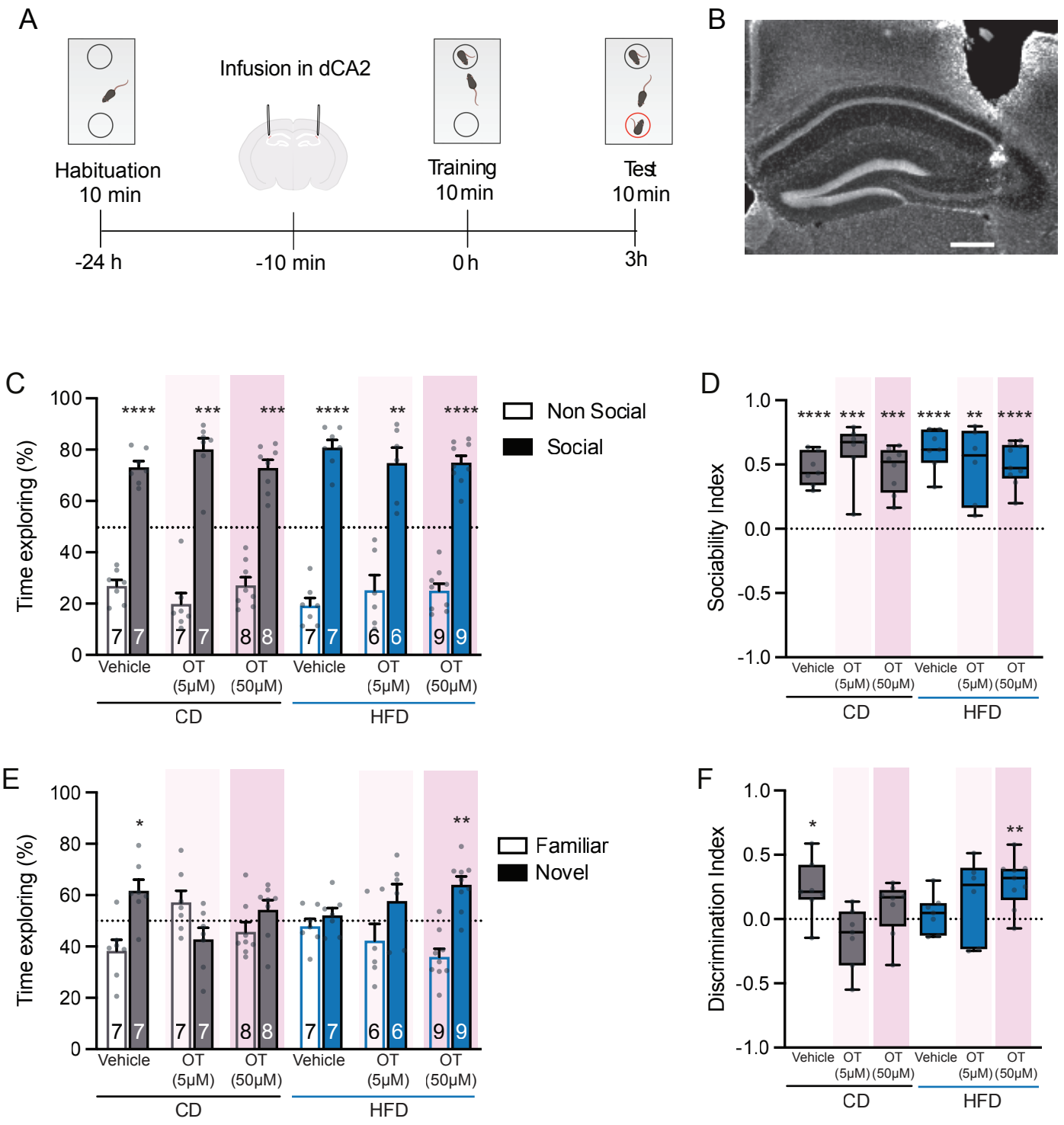
A
Infusion in dCA2
Habituation
10 min
Training
10 min
Test
10 min
-24 h
-10 min
0 h
3h
B
C
Time exploring (%)
Non Social
Social
Vehicle
OT (5μM)
OT (50μM)
CD
HFD
D
Sociability Index
E
Familiar
Novel
F
Discrimination Index

Figure 7